2019

Beyond Density Functional Theory: the Multiconfigurational Approach to Model Heterogeneous Catalysis

Samuel J. Stoneburner
Messiah University, sstoneburner@messiah.edu

Carlo Alberto Gaggioli

Christopher J. Cramer

Laura Gagliardi

Perspective article – ACS catalysis

Beyond density functional theory: the multiconfigurational approach to model heterogeneous catalysis

Carlo Alberto Gaggioli,† *Samuel J. Stoneburner,*† *Christopher J. Cramer and Laura Gagliardi* Department of Chemistry, Chemical Theory Center and Supercomputing Institute, University of Minnesota, 207 Pleasant Street SE, 55455-0431, Minneapolis, Minnesota, USA*

† C.A.G. and S.J.S. contributed equally

Abstract:

Catalytic processes are crucially important for many practical chemical applications. Heterogeneous catalysts are especially appealing because of their high stability and the relative ease with which they may be recovered and reused. Computational modeling can play an important role in the design of more catalytically active materials through the identification of reaction mechanisms and the opportunity to assess hypothetical catalysts in silico prior to experimental verification. Kohn-Sham density functional theory (KS-DFT) is the most used method in computational catalysis because it is affordable and it gives results of reasonable accuracy in many instances. Furthermore, it can be employed in a "black-box" mode that does not require significant a priori knowledge of the system. However, KS-DFT has some limitations: it suffers from self-interaction error (sometime referred to as delocalization error), but a greater concern is that it provides an intrinsically single-reference description of the electronic structure, and this can be especially problematic for modeling catalysis when transition metals are involved. In this perspective, we highlight some noteworthy applications of KS-DFT to heterogeneous computational catalysis, as well as cases where KS-DFT fails accurately to describe electronic structures and intermediate spin states in open-shell transition metal systems. We next provide an introduction to state-of-the-art multiconfigurational (MC; also referred to as multireference (MR)) methods and their advantages and limitations for modeling heterogeneous catalysis. We focus on specific examples to which MC methods have

been applied and discuss the challenges associated with these calculations. We conclude by offering our vision for how the community can make further progress in the development of MC methods for application to heterogeneous catalysis.

1. Introduction

Catalysis is fundamental to modern, sustainable chemistry and technology. A catalyst is a substance that is involved in the overall mechanism of a chemical reaction so as to lower the activation energy for the rate-determining step (referred to as the "turnover-limiting step" when the catalyst is present) relative to the situation where the catalyst is *not* present. The catalyst itself remains unchanged by the chemical reaction, and is thereby available to accelerate multiple transformations of reactants (the average number for a given reaction being referred to as the "turnover number"). Put differently, the catalyst accelerates the reaction without changing the thermodynamic equilibrium, as it remains unconsumed. Thanks to this extraordinary property, small amounts of catalyst can convert large quantities of reactants under conditions that would fail to be effective for the uncatalyzed process. Furthermore, in situations where more than one reaction product is observed (or possible) for an uncatalyzed reaction, catalysts may be designed to accelerate only those steps leading to desired products, thereby controlling selectivity.

Heterogeneous catalysts, most typically solid materials in contact with a liquid or gaseous reaction medium, are especially appealing because of their high stability and because they are relatively easy to recover and reuse—possibly after a reactivation process—which makes them an economical choice. Given these advantages, it is unsurprising that heterogeneous catalysis is ubiquitous in industrial chemical transformations.[1–3] Some examples include activation of methane by heterogeneous catalysts,[4–8] conversion of methanol to olefins,[9,10] electrocatalytic H_2 evolution,[11] oxygen evolution,[12–16] CO_2 reduction to value-added products[17–22] and biodiesel production.[23]

Modern development of catalysts tends to be bounded by two limiting approaches: the so-called "trial-and-error" procedure[24] and the "rational design" procedure.[25] Even though trial-and-error may lack a heuristic basis, it is still commonly used for catalyst discovery and development, particularly with the growing availability of high-throughput technologies that permit the efficient testing of many possibilities. The alternative, rational design of catalysts,

particularly with respect to the control of activity and selectivity, requires a thorough understanding of a given reaction mechanism[26] and often involves the discovery of structure−activity relationships involving chemical concepts and descriptors. Subsequent exploitation of such relationships facilitates the design of increasingly active catalysts, or the discovery of completely new ones. Such comprehensive and precise information, however, can be difficult to obtain exclusively from experiments because it generally requires atomic-level characterization of species that can be short-lived, e.g., high-energy reaction intermediates. Moreover, while the kinetics of the reactions can be studied by kinetic experiments,[27,28] more detailed information on the nature of associated transition states may be difficult to acquire. Computational catalysis is then a useful tool that can contribute to the mechanistic understanding[29] of catalysis through molecular and periodic (for solid state materials) simulations. Ultimately, the insights from computational studies can be used for rational catalyst design.[30] Reports of computational catalytic studies have increased exponentially in recent years,[31] and the field is sufficiently mature for the relevant techniques to be employed routinely.

In this perspective, we first address one of the most popular theoretical methods currently applied to heterogeneous catalysis, namely, Kohn-Sham density functional theory (KS-DFT;[32] abbreviated simply as DFT below, unless we have a special reason to emphasize that the typical implementation of DFT involves the Kohn-Sham approximation, which derives the density from a single-determinantal product of molecular orbitals). We then turn our attention to cases where DFT fails to provide results of acceptable accuracy owing to the limits of its applicability. The paper is structured as follows: in Section 2, we describe the state-of-the-art in modeling computational heterogeneous catalysis, particularly using DFT methods and highlighting some specific achievements. In Section 3, we present alternative examples that reveal selected drawbacks of DFT. Section 4 is devoted to reviewing MR methods, while in Section 5 we discuss some examples of MR applications to catalysis, or to systems potentially relevant for understanding catalysis. While the scope of this perspective is primarily motivated by

heterogeneous catalysis, the literature contains very few examples of multireference methods in heterogeneous catalytic studies. Therefore, in order to illustrate the possible applications of multireference methods we will also discuss a few examples of homogenous systems. Finally, in Section 6, we offer our outlook with respect to going beyond DFT in future computational catalytic studies.

2. Introduction to state-of-the-art modeling in heterogeneous catalysis

In this section we discuss selected examples of computational heterogeneous catalysis achievements featuring DFT.[32] Due to the widespread popularity of DFT for heterogeneous catalysis modeling, providing exhaustive coverage would be well beyond the scope of this work. Instead, we aim to provide a flavor of the capabilities of DFT, and direct the reader to additional specialized reviews as appropriate.

One of the greatest achievements in the field of theoretical heterogeneous catalysis and surface science has been the development of so-called scaling relationships.[33–35] Broadly speaking, these relationships constitute a series of correlations, generally linear in nature, between adsorption energies of different species across a range of catalytic surfaces. An example of such scaling relationships is provided by Latimer et al.,[7] who showed a linear correlation between DFT-calculated transition state (TS) energies for C-H activation in hydrocarbons and hydrogen-atom adsorption energies over 20 distinct active site motifs and catalysts, including materials as wide-ranging as zeolites, oxides, metals, and metal-organic frameworks (MOFs). Scaling relationships are important constructs because they correlate the chemistry of a catalytic reaction with one, or a few descriptors, thereby enabling the rapid discovery of improved catalysts when the prediction of the descriptor is more facile than computing the full catalytic reaction, which is nearly always the case. Scaling relationships elucidate reactivity trends and permit, in many cases, the construction of so-called “volcano plots”, which are representations that express the reactivity (rate of catalyzed reactions or closely related variables) as a function

of a limited number of independent descriptors. For example, Latimer et al.[7] reported volcano plots of rates of methane activation against the free energy of active site formation (G_f). Considering only metal oxides M_mO_x active sites and molecular oxygen as oxidant, G_f is defined[7] as:

$$G_f\,(M_mO_x) = G\,(M_mO_x) - (1/2)\,G\,(O_2) - G\,(M_mO_{x-1})$$

These plots are called "volcano" because of their shape, and maximum reaction rates tend to exemplify Sabatier's principle.[36] For hydrogen evolution, for example, which is a two-step reaction passing through an adsorbed intermediate, the Sabatier principle states that the adsorption energy should be neither too high nor too low. If it is too endergonic, the *ad*sorption will be slow and limit the overall rate; if it is too exergonic, the *de*sorption will be slow[11] (for a review of other concepts and tools used in both homogeneous and heterogeneous computational catalysis, see Ref. [37]). For examples of scaling relationships and volcano plots in homogeneous catalysis see Refs. [38,39].

Catalytic materials for energy-related reactions are of particular interest for our own work. Recent achievements in hydrogen production are exemplified by the work by Yan *et al.*,[40] who studied solar photocatalytic materials for water splitting (i.e., the exploitation of sunlight to convert H_2O to H_2 and O_2) using periodic DFT. The authors did a thorough screening of hundreds of transition metal oxides assessing bandgaps, band positions with respect to the O_2/H_2O and H_2/H^+ electrochemical couples, and stability in aqueous environments. After selecting $Mn_2V_2O_7$ as a possible candidate, experimental characterization verified that a stable photocurrent at high pH was obtained, in agreement with the prediction from the calculations. Another energy-relevant reaction to which DFT has been widely applied is the catalytic reduction of CO_2.[18,20–22] Jain et al. have recently reviewed DFT applied to energy-relevant materials.[41]

Metal organic frameworks (MOFs) comprise an emerging class of materials for heterogeneous catalysis.[42–45] These materials are porous crystalline solids that are composed of a

metal node and an organic linker. Among possible catalyst supports, MOFs have been increasingly studied in recent years because of their relative stability and high porosity, which make them suitable for high temperature catalytic gas-phase processes.[46,47] Furthermore, their high degree of structure tunability, due to the large number of combinations of different metal nodes and organic linkers, makes them appealing when compared to traditional metal oxides, whether as catalysts or as catalyst-supports. In recent years MOFs have found applications in a wide variety of catalytic reactions.[48–55] Reviews of computational studies focused on catalysis using MOFs are available.[56–59]

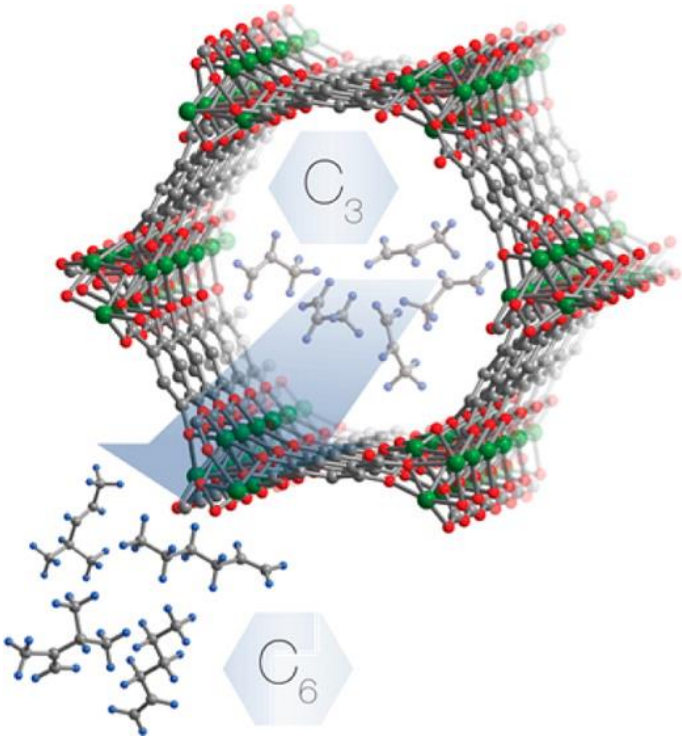

Figure 1: The MOF Ni_2(dobdc) oligomerizes propene. Reprinted with permission from Ref. [46]. Copyright 2014, American Chemical Society.

2.1. Further applications of DFT to heterogeneous catalysis

Most DFT studies in catalysis focus on computing free energies of activation, which can be related to rate constants using transition state theory.[60,61] Experiments, however, do not focus on rate constants for elementary steps, but rather on reaction rates, which depend also on concentrations and the *sequence* of elementary steps in the catalytic cycle. A useful way of introducing concentrations effects in computation is microkinetic modeling, which consists of the construction of explicit kinetic reaction networks merging the rate constants provided by calculations and concentration data supplied by experiment. The rate constants that are used for microkinetic modeling are almost always computed using DFT. Very briefly, one has to define all possible important elementary steps of the catalysis, each of which will have a standard-state reaction rate. This approach produces a system of differential equations, and the initial concentrations of all of the species can be used as starting conditions for solving these equations. With the microkinetic model, the time evolution of the concentration of each compound can be computed, and this is what most experiments measure. The use of microkinetic modeling is very important and used extensively in computational heterogeneous catalysis.[62–64]

Molecular dynamics simulations are another emerging approach in computational heterogeneous catalysis. While they are not as routinely employed as static approaches due to their high computational cost, their importance has been demonstrated for understanding the microscopic details of catalysis under realistic operating conditions (e.g., high temperatures and/or high pressures).[35,65–68] Ab-initio molecular dynamics simulations almost always make use of DFT energies and geometries for their time propagation.

Another computational advance involves the exploitation of machine learning (ML), which is emerging as an important technique in computational catalysis for predicting electronic structures, mechanisms, and outcomes of reactions.[69–78] Machine learning algorithms rely on training data as they mine correlations in order to make predictions, and the typical state-of-the-art computational method for generating training data is DFT. If DFT-generated values are

subject to large errors, any machine learning process will be unreliable, and recent work has included efforts to account for the uncertainty in the DFT data in a quantitative fashion.[69,71,72] For example, when Ulissi et al.[71] used a combination of machine learning and DFT calculations to ascertain the mechanism of the reaction of syngas on rhodium(111), they assessed the uncertainty in the DFT energies and identified additional reaction pathways that needed to be considered. After noting that at 90% confidence they could not even rule out competing products such as water and methanol, they argued that DFT uncertainty could have a large effect on machine learning attempts to elucidate mechanisms, saying "…any single mechanism derived solely from DFT calculations should be carefully checked…".[71] A detailed analysis of some of the challenges in using DFT for machine learning can be found in Ref. [78].

Despite the aforementioned challenges, machine learning has already proven its utility in heterogeneous catalyst design.[79] In order to perform simulations of systems intractably large for quantum mechanical methods, ML has been used to develop interatomic potentials (machine-learning potentials), which are functions for determining the potential energy of a collection of atoms that can then be used to evaluate interaction energies faster than DFT.[80] For example, a machine-learning potential combined with grand canonical Monte Carlo (GCMC) was able to predict the coverage of oxygen atoms on a Pd(111) surface as a function of temperature and pressure.[81] This is an important feature of machine-learning potentials because it enables sampling of the chemical space under operating conditions. At high temperatures for example, small nanoclusters can be present in many different (and possibly unintuitive) structures that would be hard or impossible to be determined without an exhaustive chemical space sampling.[82]

ML was also used in screening of Ni_xGa_y bimetallic surfaces for CO_2 reduction.[72] The exploitation of ML allowed the study of 40 surface facets and 583 different adsorption sites for CO_2 reduction catalysis. The predictions of the most active catalysts were in agreement with experimental reported activity.[83] Another noteworthy application of ML has been the study of binding energies of oxygen reduction reaction intermediates on alloys of Pt, Pd and Ni.[84] ML

with very limited DFT training data was able to predict binding energies on hypothetical alloys within 0.1 eV with respect to DFT. However, larger errors were encountered with transmutations of atoms with a charge difference greater than one, especially when the alloy component was Mn, Fe, or Zn, pointing to the need for greater accuracy in ML.

To conclude this section, we note that DFT has been, and continues to be, the most used electronic structure tool for modeling heterogeneous catalysis, and much has been accomplished thanks to its generality and versatility. For some systems, however, it has been shown that achieving chemical accuracy requires resort to a wave-function-based theory, e.g., increasing accuracy by correcting energies of reactive sites based on Møller-Plesset perturbation theory (MP2).[85–87] Additionally, error estimates (with respect to experiment) for several crystal properties as computed by solid state DFT were assessed by Lejaeghere et al.,[88] who pointed out higher errors for the description of dispersion forces, magnetic properties, and properties in general in correlation-dominated materials (such as transition metals containing systems). While in this section we focused on achievements based on DFT, in the next section we will address the other side of the coin, namely specific drawbacks of DFT when applied to the modeling of catalysis.

3. Drawbacks of KS-DFT

As discussed above, a great deal of theoretical chemistry is done using KS-DFT[32] due to its attractive balance between cost and accuracy. For many classes of problems, KS-DFT offers the most accurate results possible within the limits of computational affordability, especially for closed-shell systems. However, catalysis frequently involves open-shell systems, especially when transition-metal centers are present, and the accuracy of KS-DFT can be considerably degraded in such cases.[89] The challenges facing KS-DFT are frequently reviewed, e.g., the perspective of Yu et al.,[90] but for our purposes the most relevant are the need for broken-symmetry solutions because of multireference character,[91,92] self-interaction error (SIE),[93–101]

sometime referred to as delocalization error,[102–104] and the limited degree of universality in specific density functionals.[105] We will elaborate on each of these points in the remainder of this section.

Multireference (MR) systems are those for which more than one Slater determinant or configuration state function (CSF) is important for accurately describing the electronic structure of a specific state. Before we discuss the challenges in treating MR systems, a brief overview of "correlation" is worthwhile. Correlation is usually defined as the difference between the exact energy obtained with FCI and the simple single-reference Hartree-Fock energy,[106] and it is often divided into two categories.[107] The part associated with MR systems is usually referred to as "static" or "non-dynamic" or "left-right" correlation, i.e., the energy associated with near-degeneracy of electronic states.[107–109] In fact, the presence of static correlation defines the multireference character of a given system,[109,110] and static correlation is present in most transition metal systems of interest for catalysis.[90] Dynamical correlation arises from electron-electron interaction,[111] including short-range repulsion and long-range dispersion interactions,[110,111] and is generally more adequately addressed by DFT than is static correlation. Note that while correlation in general plays a significant role attaining chemical accuracy, the division between static and dynamical correlation is a convention developed to ease discussion, and in reality there is overlap between the two.[108,111] Nevertheless, the categories can be helpful, especially when considering which methods to use.

Large errors in DFT results are possible when studying MR systems due to the inherent single-determinant nature of the commonly employed KS formulation of DFT. Again, complexes containing transition metals (TMs) are often associated with MR character. [91,92] (For reviews of DFT accuracy analysis in transition metal complexes see Refs. [112,113].) The difficulties in treating MR systems with DFT are especially apparent for spin energetics. In KS-DFT, it is impossible to obtain a solution having the correct spin density and that is a spin eigenfunction for open-shell systems having a spin multiplicity less than the maximum $2S+1$.[89] Instead, to obtain reasonable

energetics for multireference systems, it is often necessary to use a so-called "broken-symmetry" solution that is neither a spin eigenfunction nor one that has the correct spin density. In such cases, spin contamination can become a significant problem and it can be difficult to draw conclusions about the actual spin state of a given system when employing broken symmetry methods.[90] (For additional detail regarding spin in KS-DFT, we direct readers to the 2012 review by Jacob and Reiher[89] and the 2009 review by Neese.[114]) As has been stated on many occasions, if the exact density functional were known, it would be possible to obtain exact energies even for multireference systems, but the exact functional is likely to be very complicated and completely unknowable.[90] In practice, it is necessary to use approximations, sometimes referred to as exchange-correlation (XC) functionals, or more commonly just "functionals".

Another well-known limitation of DFT is the presence of SIE, also called delocalization error, which arises from the unphysical Coulomb interaction of an electron with itself that is not completely canceled out in most commonly used XC functionals (due to the use of exchange functionals in place of the Hartree-Fock exchange in Kohn-Sham DFT).[115] This error produces an unphysical delocalization of the electrons in the molecule in order to decrease the density at any given position in space.[96,116–120] SIE can produce errors in both electron density and energy without any correlation between the two, namely a given XC functional can give correct energy but not density and vice-versa for a particular system. In this regard, Gani and Kulik noted a transfer of electrons from metals to ligands, regardless of valence orbital diffuseness, ligand electronegativity, basis set, metal, or spin state, in three strategies often employed to correct for SIE in molecular TM complexes, namely DFT+U, hybrid functionals (which include a certain percentage of exact Hartree-Fock exchange), and range-separated hybrid (RSH) functionals (which use a distance-dependent Coulomb repulsion operator and given percentages of exact Hartree-Fock exchange included only in either the short or long range portions), see **Figure 2**.[121] In contrast, when TM-containing solids were studied, Zhao and Kulik found that incorporation of Hartree−Fock exchange localizes the density away from the metal for all of the cases analyzed,

while DFT+U presents a diverging behavior, with the density moved onto the metal for low-spin and late transition metals and moved away from the metal in the other cases.[122] However, when cluster model molecular analogues were extracted from the TM solids, consistent flow of the density away from the metal was observed in all cases (irrespective of the theoretical approach). These results underline the difficulty of applying established trends for functional tuning on transition-metal complexes from molecules to solids.

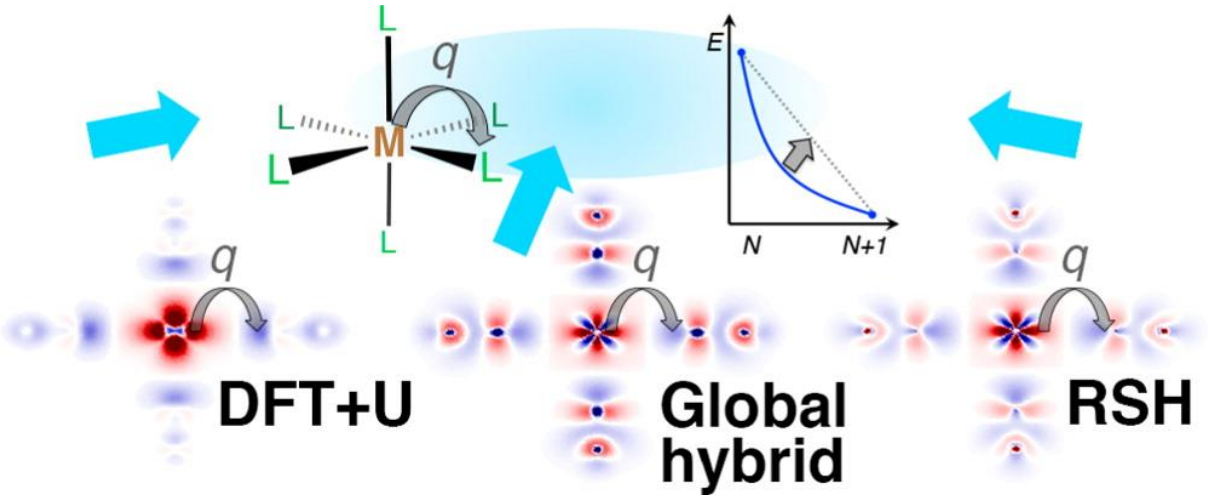

Figure 2: Charge transfer arising from different strategies to correct SIE. Reprinted with permission from Ref. [121]. Copyright 2015, American Chemical Society.

Another drawback of DFT is that it cannot capture the long-ranged electron correlation effects, also called dispersion interactions.[123] In practice, one has to resort to dispersion corrections such as the commonly used Grimme's correction,[124] although some functionals such as the M06 suite[125] account for dispersion by fitting parameters to experimental data sets that include non-covalent interactions. In contrast, most wave function theories (other than Hartree-Fock) inherently capture dispersion interactions by including in the wave function contributions generated by excitations into virtual orbitals.[123,126]

Many attempts have been made to address the above difficulties of DFT, which has resulted in a plethora of XC functionals from which to choose. While it is common practice to simply select a functional that is "popular" for a given class of systems (typically based on good past performance in analogous instances), popularity is not a guarantee of accuracy, and functionals that perform very well in some cases may do more poorly in others.

One example of the unpredictability of DFT functionals is found in a recent paper by Rugg et al.[105] in which the authors analyzed some industrially relevant catalytic reactions (hydrogenation, dioxygen activation, and methane to methanol oxidation) using multi-center cluster models of $MoVO_x$ and BiMo mixed-metal oxides with different XC functionals. These systems present challenging electronic structures for DFT; as the authors stated: "The SIE causes problems not just with *where* the electrons are localized, but *whether* they are localized at all." (**Figure 3**). The authors first tested the ability of different functionals to localize the spin density. For some of them there were dramatic differences with respect to CCSD(T)[127] reference data, not only quantitatively but also *qualitatively*, i.e., even putting the unpaired electrons on the wrong metal. Generalized Gradient Approximation functionals (GGA, namely functionals that depend on local density and its gradient) delocalize the spin density over the two metals as a result of the presence of strong SIE. The authors then analyzed the DFT reaction energies (exemplified by CH_4 activation and O_2 activation reactions over the mixed TM oxides) in comparison to CCSD(T) energies. The functionals gave varying relative energetics of reactants, products, and various intermediates, with hybrid functionals yielding results closer to CCSD(T). Notably, despite acceptable overall mean absolute deviation (OMAD) energy values for M06[125] (28 kJ/mol) and TPSSh[128] (23 kJ/mol), for some cases these functionals did not predict benchmark electron distributions. On the other hand, the range-separated functional ωB97XD[129] had the opposite problem, namely giving correct electronic structures but flawed energetics (OMAD of 41 kJ/mol). Furthermore, the authors pointed out the need for experimental reaction energies as reference data because CCSD(T) can be applied only to small systems and cannot describe

multireference systems well. Rugg et al. concluded that some functionals that work excellently for systems with only one metal[130] do not work well for complexes containing two metals[105] and emphasized that caution has to be used when choosing a functional, even when the systems under analysis are closely related to each other.

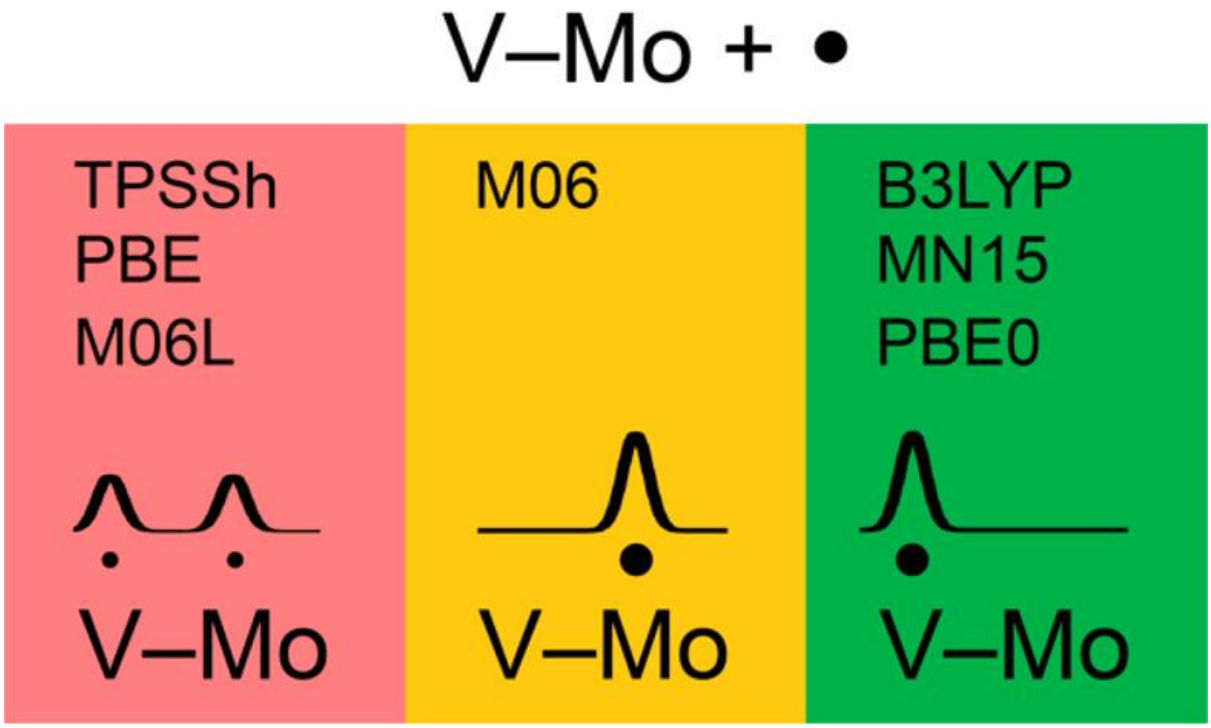

Figure 3: Electron localization variances among DFT functionals. Reprinted with permission from Ref. [105]. Copyright 2015, American Chemical Society.

In another example of DFT studies of electron localization, Asmis et al.[131] analyzed the localization (or delocalization) of electrons in vanadium oxide clusters of different sizes in gas phase ($V_4O_{10}^-$, $V_6O_{15}^-$ and $V_8O_{20}^-$) using three different functionals (BLYP,[132,133] B3LYP,[132–134] and BHLYP[133,135]) in comparison with experimental spectroscopic data. Only B3LYP was found to be able to reproduce the experimental electron localization, while BLYP gave electron over-delocalization and BHLYP electron over-localization for all the three systems. The localization of an electron hole in acidic zeolite catalysis was analyzed by Solans-Monfort et al.[136] using B3LYP and BHLYP with CCSD(T) reference calculations. BHLYP gave a localized picture in

agreement with CCSD(T), while B3LYP gave a delocalized electron hole. The amount of Hartree-Fock exchange included in the functional is therefore critical for the outcome of the calculation, and highly dependent on the system under study.

An additional example of variable DFT accuracy in catalysis is found in the work of Rozanska et al.[137] where the oxidative conversion of light alkanes by vanadium oxide catalysts were studied using DFT and CCSD(T). Interestingly, the authors found that B3LYP (which is one of the most popular functional used in catalysis) yielded larger errors than usual, -40 to -60 kJ/mol with respect to CCSD(T). With non-hybrid BP86[132] and PBE[138] functionals, the errors found were even larger than for B3LYP, and strikingly the potential energy surface is also *qualitatively* different, with the diradical intermediate formed after the C-H bond abstraction highly destabilized, which directly affects the rate determining step.

Note that the challenges we describe here in DFT energetics for transition metal systems do not preclude the use of DFT geometries single-point calculations, which is a common practice in MR wave function theory. There are numerous examples in the literature demonstrating that the DFT tends to be more robust with regards to geometry than it is with energetics. For example, a benchmarking study by Ciancaleoni et al. on intermediates in hydroamination of alkynes on gold(I) also found most functionals tested to provide accurate structures even with large and inconsistent errors in the energetic results.[139] Bühl and Kabrede found the DFT equilibrium geometries of 32 first-row transition metal complexes with several functionals and found nearly all functionals tested provided geometries in reasonable agreement with experiment.[140] However, functional dependence may be more pronounced for non-equilibrium geometries: Minenkov et al. found that internuclear distances in transition metal catalyst precursors can be overestimated in functionals that do not take dispersion into account,[141] and Simón and Goodman found that for transition state structures of organic reactions only hybrid and meta-GGA functionals yielded acceptable geometries while pure GGA functionals did not.[142]

In summary, the ability of a functional to predict the actual electronic structure, including correct spin density distribution and TM oxidation states, does not always correlate with its ability to yield good energetics by using flawed densities.[143] Most of the efforts over the years for DFT improvement have indeed been focused on energetics, considering the meeting of physical constraints of the exact functional to be a secondary problem.[144] However, DFT continues to have difficulty with correctly treating the relative energies of spin states,[145–155] which is absolutely crucial for reactivity studies, and molecular binding energies in TM complexes,[145,155] which is also of significant relevance for catalysis. For example, it is commonplace that different functionals give different answers, and that spin state ladder energies are highly dependent on the percentage of Hartree-Fock exchange in hybrid functionals.[151,153] Conversely, MR methods are generally more robust for the prediction of spin ladders and/or binding energies (when experimental data are available), even though CASPT2[156,157] (complete active space second-order perturbation theory, a method widely used to recover dynamic correlation in MR techniques) can overstabilize high spin states relative to lowest ones by up to 10 kcal/mol (see section 4).[154] Sometimes GGA functionals do yield results in agreement with MR methods, but often this is due to fortuitous cancellation of error.

4. Multireference Methods

There are a variety of methods that use multireference wave functions, and many reviews and other texts (e.g., Refs. [158–161]) are available that explain the details of these methods and the differences between them. In this work we focus on methods that have been recently applied to catalysis and related problems. All of the methods we discuss fit within the framework of configuration interaction (CI), so we will begin with a brief introduction to the method.

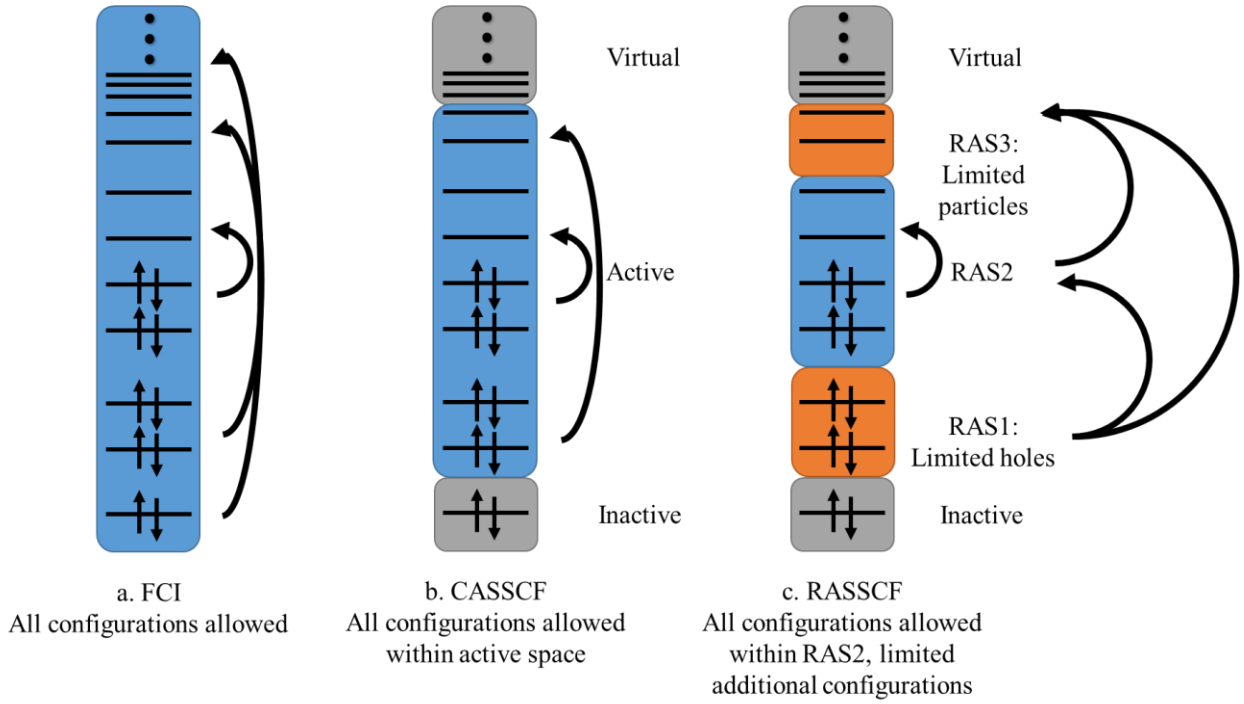

Figure 4: Active space schemes. a.) Full configuration interaction (FCI), in which all configurations are allowed within spin and spatial symmetry constraints. b.) Complete active space self-consistent field (CASSCF), in which FCI is performed only on a limited active space of orbitals, with inactive orbitals held doubly occupied and virtual orbitals held unoccupied. c.) Restricted active space self-consistent field (RASSCF), in which the active space is further divided into three subspaces, with limited excitations permitted out of RAS1 and into RAS3, but with FCI performed on RAS2.

In a full configuration interaction (FCI) wave function (**Figure 4a**), all arrangements of electrons (i.e., electronic configurations) that are possible within given user-defined spin and spatial symmetry constraints are considered. The FCI wave function is a linear combination of all permitted configurations. At the complete basis set limit, FCI yields exact Born-Oppenheimer, non-relativistic electronic energies,[106,158] but the computational expense is unfeasible for all but the smallest of systems.[158] In practice, therefore, one must select an approximation that can capture the most important configurations at a small fraction of the computational cost of FCI. For our immediate purposes, the most important two approaches are active space-based methods and excitation-based truncation. In both cases the spin- and spatial-symmetry constraints are retained, resulting in wave functions that are spin eigenfunctions and avoid the difficulties with spin contamination and broken-symmetry solutions discussed above. Other approaches include full CI quantum Monte Carlo,[162] heat-bath CI,[163] Λ-CI,[164] and adaptive sampling CI,[165] as well as many other variants that focus on selecting specific configurations or determinants, but to our knowledge they have not been applied to catalysis and we will not discuss them further.

In active space CI, most configurations are excluded by keeping many low-energy orbitals doubly occupied and most of the high-energy orbitals unoccupied. The spaces of fixed doubly occupied and unoccupied orbitals are typically referred to as “inactive” and “virtual”, respectively. The remaining orbitals are “active”, and their treatment depends on the specific form of theory in use. In the most common variety, complete active space self-consistent field (CASSCF)[166] (**Figure 4b**), FCI is conducted on all of the active space orbitals. Because of the constraints imposed by the active space selection, the computational cost of CASSCF is much less than for a true FCI calculation. Even so, the dimension of the CI problem scales exponentially with the number of electrons and orbitals in the active space, and active spaces larger than eighteen electrons in eighteen orbitals, or (18,18), are still impossible for most computers,[167] although twenty electrons in twenty orbitals has been achieved using massive

parallelization.[168] This limit can be increased significantly by the use of restricted active space self-consistent field theory (RASSCF)[169] (**Figure 4c**), which breaks the active space into three subspaces. The first subspace, RAS1, contains doubly occupied orbitals, with excitations into RAS2 or RAS3 permitted up to a user-defined maximum. Similarly, RAS3 contains unoccupied orbitals and can have excitations from RAS1 or RAS2 up to a user-defined maximum. RAS2 orbitals undergo FCI, similar to the active space of CASSCF. Because the number of RASSCF configurations is much more limited than for a CASSCF active space of the same size, it is possible to calculate larger active spaces with RASSCF than with CASSCF. Among the same family of methods, it is also worth mentioning the generalized active space SCF (GASSCF) method,[170] the occupation-restricted multiple active space (ORMAS) method,[171] generalized valence bond (GVB),[172] and the separated pair (SP) approximation.[173] In these approaches different constraints are followed to divide the active space in subspaces and control the number of CSFs in the CI expansion. Their utilization in catalysis has been limited because of the challenge of selecting an active space or a partition of excitations. We will discuss this problem further in Section 6.

Even larger active spaces may be treated using density matrix renormalization group theory (DMRG).[174–176] DMRG restates the FCI wave function in terms of orbital occupation numbers and decomposes the corresponding FCI tensor into a contracted matrix product state (MPS). For most practical applications the product expression is truncated based on an arbitrarily chosen "bond dimension",[177] sometimes labeled "D"[177] or "M".[178] The truncation of the CI matrix product expression provides much of the advantage in computational effort when using DMRG methods. While this truncation could be seen as similar to the truncation of the FCI summation expression in conventional active-space or excitation-based CI methods, it is important to understand that the product truncation in DMRG is not restricted to excitations of a given rank, and in principle all of the FCI coefficients can be treated. However, unless M is very high, orbital selection and ordering can play a significant role in the results, which is not the case

for true FCI. Moreover, it is common to impose additional restrictions analogous to CASSCF by restricting certain orbitals to being doubly occupied or unoccupied. Because the matrix product truncation provides significant savings compared to a true FCI calculation even when performed only for an orbital active space, much larger active spaces can be considered. Currently up to 84 electrons in 84 orbitals (84,84) has been performed,[179] and over 100 active orbitals are feasible.[180]

In all of the cases discussed above, only part of the correlation energy is included. In CASSCF and other active-space methods we have discussed, static correlation is fully recovered so long as the active space is properly chosen, that is, so long as only configurations of very small weight are excluded. However, choosing the active space is not simple or straightforward, and generally it is necessary to manually select individual orbitals based on chemical intuition and trial and error.[181] Work is ongoing in several groups to minimize this obstacle (e.g., Refs. [181–183]), which will be addressed in more detail in the "Outlook" section.

Even with a good active space, the results will be only qualitatively correct, as the exclusion of low-weight configurations prevents full recovery of dynamical correlation. An additional calculation step is required to get energies with quantitative accuracy, which is necessary for comparison to or prediction of experimental values, or when using these multireference calculations to benchmark other methods such as KS-DFT functionals. Increasing the active space size will include ever-increasing amounts of dynamic correlation, but capturing all dynamical correlation would, in principle, require including all remaining configurations, i.e., FCI, which as stated above is unaffordable. However, there are several strategies for including enough additional configurations such that the dynamical correlation can be approximated. The most popular[184] method to follow-up CASSCF, RASSCF, GASSCF, or DMRG-CASSCF calculations is second-order perturbation theory (CASPT2,[156,157] RASPT2,[185] GASPT2,[186] and DMRG-CASPT2,[187] respectively). Using the CASSCF wave function as its zeroth-order reference wave function, CASPT2 determines the second-order energy from the first-order wave

function, which it obtains by projecting single and double excitations from the reference wavefunction onto a modified zeroth-order Hamiltonian. In most calculations the Hamiltonian is modified with a level shift known as IPEA in order to correct for an inherent error in CASPT2 that underestimated bond energies due to inconsistent treatment between closed-shell and open-shell cases. The term "IPEA" arises because the original derivation of the shift was an attempt to obtain correct ionization potentials (IP) and electron affinities (EA). Note that the IPEA shift is therefore an empirical parameter, with a standard recommended value of 0.25 hartrees.[188] The user can set other values of the IPEA shift in an attempt to obtain better agreement with experiment for their own systems of interest, but doing so reduces CASPT2 to a semi-empirical method and we do not endorse this as a general practice. The use of IPEA is a matter of ongoing debate, with some saying it should not be used at all,[189] while others embrace it as an empirical parameter,[190] and others recommend the default value only.[191] In the latter case, Pierloot et al. specifically discussed high-spin bias in CASPT2, assigning it to inconsistent treatment of core orbitals in first-row transition metals.[191] CASPT2 also suffers from an "intruder state" problem, in which at particular points on a potential energy surface can have an erroneously large contribution from certain configurations due to near-zero values in the energy denominator. This can often be resolved by the application of an imaginary level shift to the denominator.[192] Finally, the computational cost of CASPT2 for large active space sizes is even greater than for the preceding static correlation step due to the need to calculate higher-order (up to fourth) reduced density matrices that scale as poorly as N^8, where N is the number of active orbitals.[187,193,194] The CASPT2 step in a CASSCF/CASPT2 calculation begins to dominate timing and memory requirements at about fourteen electrons in fourteen orbitals (14,14),[193,194] making it impractical for active spaces with more than 14 orbitals,[187] despite CASSCF calculations of (18,18) active spaces being possible.[167] Even DMRG-CASPT2 is feasible only for up to 30 orbitals,[187] in contrast to 100 or more for the DMRG step.[180] A different method, n-electron valence state perturbation theory at second order (NEVPT2),[195] achieves greater computational efficiency through the use of an alternative zeroth-order Hamiltonian and varying

contraction schemes, and it has also been paired with DMRG.[196] NEVPT2 does not require energy shifts for IPEA and does not suffer from the problem of intruder states,[195] but it has been noted that it has large errors in the calculation of relative spin energetics for transition metal complexes.[191]

Another approach to recover dynamic correlation is multireference configuration interaction (MRCI).[197–199] Rather than treating additional configurations perturbatively, MRCI calculates excitations explicitly from a multireference wave function such as CASSCF. While CASSCF features FCI on a limited set of orbitals, MRCI adds additional configurations defined by specific classes of excitations (i.e., singles, doubles, etc.). In this regard, MRCI has analogies with the single-reference method referred to simply as CI, with the difference being that CI uses a single-reference wave function such as Hartree-Fock, while MRCI uses a multireference wave function such as CASSCF. MRCI with sufficiently high excitations (typically singles and doubles, i.e., MRCISD) is considered to be a very high quality method and is sometimes used as a benchmarking tool (e.g., Ref. [200]). A noteworthy variant of MRCISD is averaged coupled-pair functional (ACPF),[201] which attempts to correct the formal problem of size-extensivity. However, much like CASPT2, MRCI requires fourth-order reduced density matrices, and has similar scaling limitations. Using DMRG-MRCI, active spaces as large as (29,29) have been reported.[202]

Alternative options for recovering dynamical correlation at low cost are in development, including multiconfiguration pair-density functional theory (MC-PDFT).[203] MC-PDFT recovers both static and dynamic correlation by applying an on-top density functional to density and on-top pair density (associated with the probability of finding two electrons in a given location) matrices obtained from a multi-reference wave function calculation such as CASSCF. Energies are calculated by taking the kinetic energy and classical Coulomb contributions to the wave function energy and adding them to the exchange and correlation calculated by the on-top density functional. (This partitioning of the energy is a departure from the many previous

attempts to combine MR wave function theory with DFT, motivated in part by the need to avoid double-counting of dynamic correlation energy. Interested readers are directed to Ref. [110], particularly section II.C. and associated references.) Because the wave function that provides the densities is constructed as a spin eigenfunction, no spin contamination is present, nor are broken-symmetry approaches needed.[204] Similarly, MC-PDFT does not have the SIE (or delocalization error) found in KS-DFT, provided that certain conditions are met regarding the degree of spatial symmetry imposed by the preceding wave function theory calculations.[205] MC-PDFT has been applied to a variety of transition metal compounds, including MnO^{4-},[206] $Re_2Cl_8^{2-}$,[207] ferrocene,[193,194] and others.[208–212]

The combination of MC-PDFT with DMRG (DMRG-PDFT) was recently developed and demonstrated on the singlet-triplet gaps of polyacenes and polyacetylenes with active spaces as large as (30,30),[178] and another study on iron porphyrin included a (34,35) active space for DMRG-PDFT.[213] Additionally, DMRG-PDFT is comparable to DMRG alone in terms of computational expense,[178] unlike the CASPT2 portion of DMRG-CASPT2,[187] and thus DMRG-PDFT could theoretically be applied to any active spaces that can be affordably treated with DMRG alone (i.e., over 100 active orbitals[180]). Additional ongoing developments in MC-PDFT and other CASSCF-related methods are discussed in the Outlook.

5. Applications of Multireference Methods for Catalysis

While current KS-DFT XC functionals are sometimes, if inconsistently, able to get reasonable results for multireference systems despite the single-reference nature of DFT, formally multireference methods have rarely been applied to full catalytic systems. When multireference methods are used at all, they are typically on small model systems. They usually address only one particular question about the catalytic system, and are often used primarily as benchmarking tools for the selection of KS-DFT functionals (e.g., Refs. [200,214]). We present some examples here, but they should not be taken as an exhaustive list, as it is possible for a given work to have some relevance to catalysis even if the primary motivation was a different application. For example, in a study of metalated catecholates for gas separations on MOFs,[215] DFT and CASPT2 results suggested the possibility of N_2 activation due to back-binding.[215] Using active spaces that included the 3*d* orbitals on the metal, the 2*p* orbitals of the N_2, and the delocalized π orbitals on the carbon ring of the catecholate, CASSCF orbital occupancies showed that with N_2 bound in an end-on fashion to the low-coordinate metal center, the 3*d* orbitals of the metal interacted in a π/π* fashion with the π* orbitals of the N_2. Such activation could prove useful in ammonia synthesis.[215]

As this perspective is primarily motivated by heterogeneous catalysis, most of the references we discuss in this section are on models of heterogeneous catalytic systems. However, we include a few examples of homogenous systems that serve as good illustrations of how multireference methods can be used in catalysis. Additional examples of multireference calculations on homogenous catalysts or enzymatic systems can be found in Refs. [216–227].

An especially good example of the detailed analysis possible with multireference wave function theory can be found in the work of Kurashige et al.,[228] in which they studied the mechanism of O-O bond formation in oxygen evolution from water with a K_2FeO_4 catalyst dimer. Using geometries obtained with B3LYP[132–134] on a gas-phase $[H_4Fe_2O_7]^{2+}$ cluster model, they employed DMRG-CASPT2 and DMRG-MRCI with a (36,32) active space along with

CASSCF/CASPT2 and CASSCF/MRCI with (4,4) and (20,14) active spaces for both. The (36,32) active space consisted of the ten Fe 3*d* orbitals, two 2*p* orbitals for each of the O atoms, and the third 2*p* and a 2*p*' "second-shell" orbital for the two O atoms associated with the O–O bond formation. The (20,14) active space primarily had the 3*d* orbitals of the Fe atoms and 2*p* orbitals from the O–O oxygens. (No information was provided regarding the nature of the (4,4) orbitals.) They also performed single-point DFT calculations with TPSSh,[128] CAM-B3LYP,[229] and BP86.[132,230] Qualitative agreement was found among all DMRG calculations inasmuch as they all predicted the activation energy to be positive and the reaction energy to be negative or close to zero. Quantitative results, however, differed significantly. The inclusion of dynamic correlation in the DMRG calculations (whether CASPT2 or MRCI) lowered the activation barrier from the DMRG-CASSCF value by about 5 kcal/mol, but the reaction energy was lowered (by 4 kcal/mol) only with DMRG-MRCI. The hybrid-functional DFT energies of the product were about 9-13 kcal/mol lower than DMRG-CASPT2 and 5-10 kcal/mol lower than DMRG-MRCI, differences that would make the O_2 release step noticeably less likely in the DFT predictions. The CASSCF calculations were found to have insufficiently small active spaces, as the (4,4) calculations leading to unphysical predictions and the (20,14) active space results agreed with DMRG only for the reactant-to-transition-state portion of the reaction (with a 15 kcal/mol difference for the product energy between CASSCF (20,14) and DMRG-CASSCF). However, both CASSCF (20,14) and DMRG-CASSCF natural orbital occupation numbers (NOONs) were in reasonable agreement and were used for qualitative analysis of the electronic structure during O-O bond formation. In departure from previous studies, which had predicted the product intermediate to have a single O-O bond and two Fe(V) centers based on single-reference methods, Kurashige et al. found that the O-O bond order would be 1.5 and that the Fe oxidation state would be +4.5. They pointed out that these conclusions were possible only because of the multi-reference approaches they used.

In order to better understand oxygen activation on iron for catalytic purposes, Maier et al. studied the vibrational spectrum of FeO_2^+ with infrared photodissociation experiments (using complexes with He) and at several levels of theory, including DFT, CASPT2, and MRCI.[200] The use of a small model system allowed them to perform higher-level theory than would have been possible on a real heterogeneous catalysis material. Relative energies of different spin and spatial symmetry states at several different geometries were calculated, using MRCI with singles and doubles (MRCISD) as a reference after estimating correction terms to account for higher excitations, active space size, core-valence interaction, basis set size, and scalar relativistic effects. No methods yielded the same state ordering as the corrected MRCI results, mainly due to large variations in the results for the "inserted" complex featuring the Fe atom between the oxygen atoms. The best agreement with the MRCISD reference was provided by ACPF, followed by CASPT2. The authors defined multiple active space choices, with their minimal (15,11) active space having the Fe 4*s* and 3*d* orbitals and the O 2*p* orbitals. They also indicated the use of two different (15,12) active space and a (15,13) without specifying the nature of the additional orbitals, noting that the (15,13) could be performed with CASPT2 but not MRCI. (Note that the authors used a different labeling convention in which (N_1,N_2) refers to the number of orbitals in A" and A', but the numbers we present are in the more common notation where (n,N) refers to the total number of active electrons and orbitals, respectively). The authors estimated the effects of using the smaller active space to be limited compared to most of the other corrective terms, although corrections were as large as 20 kJ/mol and they had to exclude octet states from analysis because the active spaces were not big enough. Basis set effects were also declared to be small, albeit with correction terms up to 33 kcal/mol. None of the DFT functionals studied (PBE,[138] BP86, [132,230] TPSS,[128] B3LYP, [132–134] TPSSh,[128] and B2PLYP[231]) were found to yield quantitatively accurate results, with mean absolute errors of 17-70 kJ/mol and all functionals having individual errors over 120 kJ/mol. Spin contamination was observed to affect the qualitative descriptions as well, with doublet states having spin density on oxygen atoms in DFT results but not in CASSCF results. Assignment of the experimental IR spectra was

conducted based on the corrected MRCI results, finding that two isomers contributed to the experimental bands: Fe^{V} in an inserted complex and Fe^{II} in a side-on structure.

Vanadium oxide clusters have also been studied as models for heterogeneous catalysis systems. Pykavy et al.[232] calculated potential energy curves for monocationic, neutral, and monoaniaonic states of $V_2O_4^{+/0/-}$ using CASSCF-ACPF and DFT, specifically, the B3LYP[132–134] functional. They found B3LYP to be sufficient for structures, spin state relative energies, the ionization potential, and the electron affinity, with errors of about 0.2 eV or less even with strong MR character in the neutral and anionic molecules. However, barrier heights had errors as large as 30 kJ/mol (over 0.3 eV), and, citing nonsystematic errors in B3LYP energies in general, the authors recommended that future work with multiple transition metals use ACPF single-point calculations on DFT-optimized structures. The CASSCF-ACPF calculations were performed with two active spaces, one of which featured any orbitals that were singly occupied in high-spin Hatree-Fock calculations (primarily V 3*d* orbitals) and a larger one that included four, four, and six V 3*d* orbitals for the cation, neutral molecule, and anion, respectively, along with four O 2*p* orbitals. The authors note that even the larger active space may not be sufficient for the relative spin energetics, but their larger active space results were in close agreement (0.02 eV) with experiment for the vertical electron detachment energy of the anion.

Vanadium oxo complexes, including a V^{III} case, were studied by King et al.[233] as model systems for understanding possible oxidation states for both homogeneous and heterogeneous catalysis. The work featured experimental synthesis and characterization of several complexes in an attempt to obtain low oxidation states of vanadium in supported vanadium oxo species, followed by theoretical studies of the electronic structures with DFT and CASSCF/NEVPT2 using an active space consisting of the five V 3*d* orbitals. Reacting $[V^{IV}(O)(PY5Me_2)](OTf)_2$, where ($PY5Me_2$) = 2,6-bis[1,1-bis(2-pyridyl)ethyl]pyridine and ($^{-}OTf = {}^{-}OSO_2CF_3$), with cobaltacene yielded $[V^{III}(O)(PY5Me_2)]OTf$, which was reported as the first case of a single-metal $[V^{III}(O)]^{+}$ species. Electrochemical results suggested that it might be possible to reduce the

vanadium further to [V^{II}(O)PY5Me_2], but attempts to do so were unsuccessful. CASSCF/NEVPT2 and DFT results predicted that [V(O)PY5Me_2], the complex that was the target for a V^{II} oxo species, would instead have higher oxidation states due to charge transfer to the pyridine ligands via π interaction. However, CASSCF and DFT disagreed as to the degree of oxidation: CASSCF predicted a one-electron transfer leading to V^{III}, while DFT predicted two-electron transfer and V^{IV} (**Figure 5**).

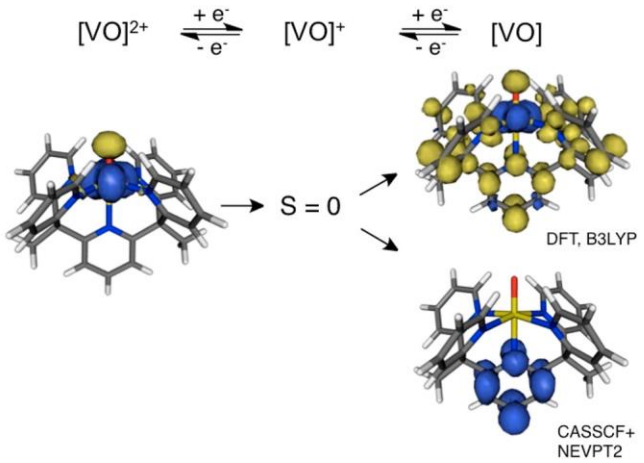

Figure 5: Predicted spin density of vanadium oxo species. Reprinted with permission from Ref. [233]. Copyright 2014, American Chemical Society.

The oxidation of methane to methanol is an especially high-value catalytic target, and inspired by enzyme active sites Rezabal et al.[234] studied the differences between CuO^+ and $CuOH^+$ for C-H activation of methane. While they primarily used DFT (B3LYP, [132–134] M06,[235] and B38P86[236]) with a CCSD(T) reference, the singlet reaction pathway of CuO^+ was found to be multireference in character and they chose CASPT2 their reference method in that case. The active space included Cu 3*d* and "second shell" 3*d'* orbitals, O 2*p* orbitals, and "relevant" orbitals from the methane molecule. Geometries for all species were optimized with B3LYP. They noted that the DFT results all had large deviations from the CASPT2 results, with maximum deviations of 16.7, 9.4, and 16.7 kcal/mol for B3LYP, M06, and B38P86. CASPT2 also predicted the

reaction to be more exothermic than CCSD(T) did by predicting higher energy for the reactants by 14.7 kcal/mol and lower energies for the final intermediate by 7.4 kcal/mol. However, they did not perform CASPT2 on any of the cases other than the singlet CuO^+ pathway based on their T diagnostics yielding single reference values, so it is not known if there would have been better agreement between CASPT2 and CCSD(T) in those cases. Except for one intermediate, the triplet reaction path was predicted to be ground by all methods, however, and after calculating the CASSCF spin-orbit coupling constant to be 1.2 cm^{-1} the authors concluded that the system is highly unlike to change its spin state.

Activation of C-H bonds has also been a major feature of MR theoretical work directly inspired by hetereogeneous catalytic systems such as zeolites. Vogiatzis et al.[237] studied methane to methanol on a $[Cu_3(\mu\text{-}O)_3]^{2+}$ cluster as a model of a possible active site in mordenite. Earlier work had indicated that metal-to-ligand charge transfer should be relevant, but it was unclear whether the Cu centers were 2+ or 3+. Accordingly, they used DFT, CASPT2, and RASPT2 to study the oxidation states of the Cu centers, the Cu-O bond orders, and the ground spin state of the overall cluster. One of the especially nice features of this paper is that it includes a systematic exploration of the active space in the supporting information. The authors found that the multireference character of the $[Cu_3(\mu\text{-}O)_3]^{2+}$ cluster came from only five orbitals with occupation numbers between 0.04 and 1.96 (**Figure 6**) and that the doubly occupied Cu 3*d* orbitals did not participate in binding with the μ-O atoms and could be disregarded. However, progressively adding μ-O 2p and 3p orbitals led to CASSCF spaces of (11,11), (13,13), and (15,15), and eventually a RASSCF space of (19,21) with RAS2 consisting of the minimal five orbitals. The (5,5) active space was deemed insufficient because CASPT2 relative spin state energies disagreed significantly with the CASPT2 and RASPT2 results using other active spaces, as well as with other methods. The CASSCF (11,11) and RASSCF (19,21) active spaces were chosen to be reported in the main manuscript, although it should be noted that an earlier CASSCF (11,11) calculation had very different relative spin results from the one reported in the

manuscript, which the authors attribute to the use of the RASSCF (19,21) orbitals as the initial guess for the orbitals in the (11,11) calculation reported in the paper. This discussion reflects the importance of the initial guess in MCSCF calculations. Both CASPT2 (11,11) and RASPT2 (19,21) predicted the spin state to be a doublet, with the quartet over 20 kJ/mol higher. However, the two methods disagreed regarding the degree of the doublet-sextet gap, with CASPT2 predicting 78.1 kJ/mol and RASPT2 predicting 108.6 kJ/mol. In the ground state configuration, one Cu atom was pure d^9, as expected for Cu^{II}, while the other two were of mixed $Cu^{II/III}$ character as they shared electrons with two of the oxygens through σ interactions. Those oxygens were of radical oxyl character, while the remaining oxygen was oxo (2-). Calculation of excited states revealed a low-lying (18 kJ/mol above ground) configuration in which one of the radical oxygens took on the oxo character and the oxygen that had been 2- became oxyl. The remaining oxygen retained oxyl character in both states, and was also the one with best accessibility for methane once the environment of the zeolites walls were taken into account. Periodic DFT confirmed that this radical-oxyl oxygen was favored for hydrogen transfer from methane, with an activation barrier of 37 kJ/mol, while the two oxygens that could be found in oxyl or oxo forms had activation barriers of 74-78 kJ/mol.

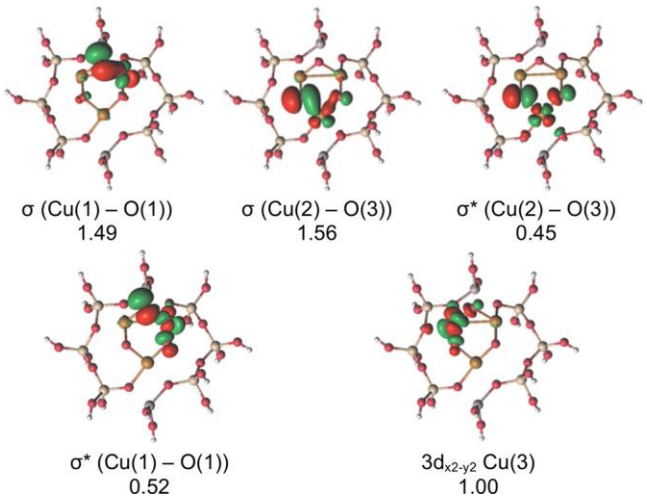

Figure 6: Key molecular orbitals of $[Cu_3(\mu\text{-}O)_3]^{2+}$ cluster, doublet spin state. Reprinted with permission from Ref. [237]. Copyright 2017, American Chemical Society.

Iron-containing zeolites have also been studied for methane activation using multireference methods. Snyder et al.[238] used CASPT2 on DFT-optimized structures in combination with magnetic circular dichroism on the Fe(II)-beta (BEA) zeolite (featuring iron atoms supported by an aluminosilicate framework) to study the α-Fe(II) active site and the associated α-O intermediate in methane to methanol conversion. Computational efforts were of interest because α-Fe(II)-containing zeolites also have many other "spectator" species that make it difficult to assign features in experimental spectroscopy. The authors chose to study α-Fe(II) in BEA based on their new discovery of spectral features that were most intense for this particular case. In particular, they observed a weak ligand-field band in diffuse reflectance ultraviolet-visible (DR-UV-vis) at 15,900 cm^{-1} that was replaced by a feature at 16,900 cm^{-1} after N_2O activation. The authors assign the 16,900 cm^{-1} feature to the α-O intermediate, as it disappeared after reaction with CH_4. Magnetic circular dichroism (MCD) and Mössbauer data indicated the α-Fe(II) site was square planar and mononuclear with a positive zero-field splitting (ZFS) leading to $S = 2$. After identifying possible motifs within the BEA framework that would be compatible with such an iron site and would be accessible to CH_4, the authors found that there could be multiple arrangements of two aluminum and four silicon atoms and employed computational methods to understand the effects. Using an active space consisting of the five Cu 3*d* and five Cu 3*d′* "second-shell" orbitals and the bonding O 2*p* orbitals, they found that CASPT2 could reproduce the positive ZFS of the experimental work only if the aluminum atoms each lay across from each other between two oxygen atoms bound to the iron. Based on CASPT2 results, the 15,900 cm^{-1} band of α-Fe(II) was assigned to a $3d_{z^2} \rightarrow 3d_{x^2-y^2}$ transition. The authors note this transition is of high energy in part because the $3d_{z^2}$ orbital is stabilized by mixing with 4*s* due to the lack of axial ligands.

A follow-up study by Hallaert et al.[239] added considerable detail as it further addressed Fe(II)-BEA along with two other zeolites, ZSM-5 and ferrierite. Ligand field (LF) spectra were calculated with CASSCF/CASPT2 (**Figure 7**). Setting the same types of Cu and O orbitals for

the active spaces as in the previous work by Snyder et al.,[238] the authors concluded that for all three zeolites studied, CASPT2-calculated $3d_{z^2} \rightarrow 3d_{x^2-y^2}$ transition energies could reproduce DR-UV-vis bands around 16,000 cm^{-1} only for the same arrangement of aluminum and silicon found by Snyder et al.[238] for Fe(II)-BEA, i.e., with two Al atoms distributed symmetrically across the six-membered ring from each other, and at the sites on the ring that provide minimal Al-Al distance. (We follow the nomenclature of the authors in this and the following related papers by using "six-membered ring" to refer to rings of twelve atoms: six oxygen atoms alternating with Si or Al atoms.) CASPT2 was also used to investigate a disagreement between periodic PBE[138] and cluster calculations using B3LYP[132–134] regarding the level of coordination of certain types of Fe sites (labeled γ) in Fe-ZSM-5. The periodic PBE calculations predicted 4-fold coordination to be the most stable, while cluster B3LYP predicted 6-fold coordination. CASPT2 using the B3LYP structures predicted a difference between 4-fold and 6-fold coordination of about 1 kcal/mol, so the authors concluded that the differences were a matter of functional dependency rather than the use of cluster or periodic models. Having noted the importance of the α-Fe site being in square-planar geometry, the authors also compared square-planar geometries with tetrahedral using DFT and CASPT2 in order to confirm their hypothesis that the square-planar geometry is not forced by the zeolite framework. Considering several points along a dihedral angle (δ) coordinate between the two FeO_2 triangles, they found that CASPT2 favored square-planar slightly more than DFT, with minima at $\delta \approx 35°$ and 45°, respectively (**Figure 8**). They estimated the geometric strain imposed by the zeolites to obtain an "ideal" square-planar structure to be no more than 1 kcal/mol. The square-planar electronic structure was predicted by CASSCF to include a doubly occupied $3d_{z^2}$ orbital and four singly occupied 3*d* orbitals. They suggested the $3d_{z^2}$ orbital benefits from additional stabilization through mixing with the 4*s* orbital, which they expected would strengthen the Jahn-Teller effect that was taken to be the main cause of the stability of the square-planar structure.

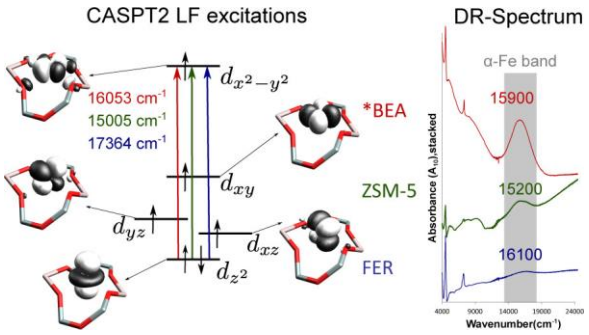

Figure 7: Ligand-field excitations of α-Fe calculated by CASPT2 and corresponding experimental DR-UV-vis absorbance bands. Reprinted with permission from Ref. [239]. Copyright 2017, American Chemical Society.

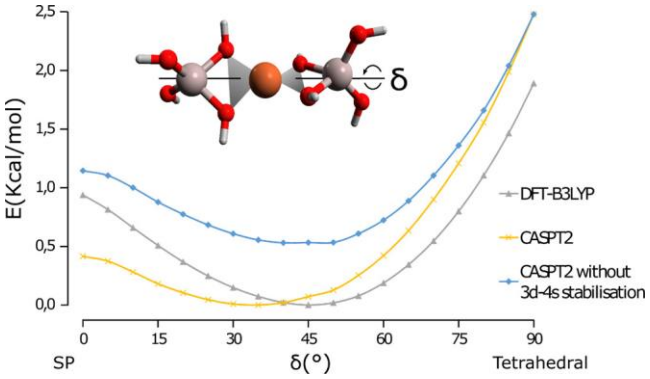

Figure 8: Energies of α-Fe with varying ligand oxygen dihedral angles calculated with DFT and CASPT2. Reprinted with permission from Ref. [239]. Copyright 2017, American Chemical Society.

Yet another zeolite, Fe-CHA, was examined for methane activation by Bols et al.[240] As in the previous two papers (and using the same type of active space), CASPT2 LF spectra confirmed that the α-Fe was in a six-membered ring with two Al across from each other, with CASPT2 transitions at 4065 and 13,478 cm^{-1} and experimental DR-UV-vis-NIR (NIR = near infrared) spectroscopy yielding 5400 and 13,000 cm^{-1}, respectively. The CASPT2 calculated *d* transitions were also compared among Fe-CHA and several previously studied zeolites to confirm the DFT findings that CHA had weaker Fe binding than the other cases (38 kcal/mol lower than BEA), which the authors said could lead to deactivation of Fe-CHA through migration of the Fe cation under reaction conditions.

Many of the studies of heterogeneous catalysts featuring multireference treatment have been on metal-organic frameworks. The MOF-74 family, especially Fe_2(dobdc) and $Fe_{0.1}Mg_{1.9}$(dobdc), drew a good deal of attention after Xiao et al. reported its conversion of ethane to ethanol.[241] Verma et al. continued the investigation into the specific mechanism of ethane conversion (**Figure 9**) using DFT and CASPT2.[242] CASPT2 treatment was applied to two specific structures: the **B′** iron(IV)−oxo intermediate (where **B′** is **B** with the N_2 removed) and the **TS2** hydrogen atom abstraction transition state. For **B′** the authors used a (18,12) active space that included the Fe 3*p* core orbitals, the Fe 3*d* orbitals, and O 2*p* orbitals as needed for the bonding/antibonding interactions with the Fe 3*d* orbitals. For **TS2**, a (12,11) active space was used that consisted of the five Fe 3*d* orbitals, one of which was in a σ/σ* bonding/antibonding interaction with the evolving –OH group, and three O 2*p* and two O 3*p* orbitals. In both cases a smaller 26-atom cluster was cut from the 88-atom cluster model used for DFT; this choice was validated by different cluster comparisons provided in the supporting information. They concluded that a high-spin iron(IV)−oxo complex played a key role in the catalytic conversion of ethane, and in contrast to previous work on nonheme iron(IV)-oxo species, they found that the reaction path should proceed entirely along a quintet ground state with no spin flip, particularly as both CASPT2 and M06-L predicted large gaps between the quintet and septet or triplet states for **TS2**. CASPT2 on **TS2**-based structures also played a key role in determining the relative likelihood of a *σ*-electrophillic attack leading to catalytic reactivity and a *π*-electrophillic attack leading to self-decay. Verma et al. found that the *σ*-channel was determined to be more favorable by 24.3 kJ/mol, establishing the favorability of the catalytic pathway. Their work inspired a computational screening[243] performed by Vogiatzis et al. on a database of experimental MOF structures to find other MOFs that could support such a system, with experimental work was performed on the most promising candidates. Additionally, screening of possible ligands in search of additional variants of the Fe site was conducted by Liao et al. using DFT,[244] with their choice of the M06-L functional justified by the agreement with CASPT2 results in the work of Verma et al.[242]

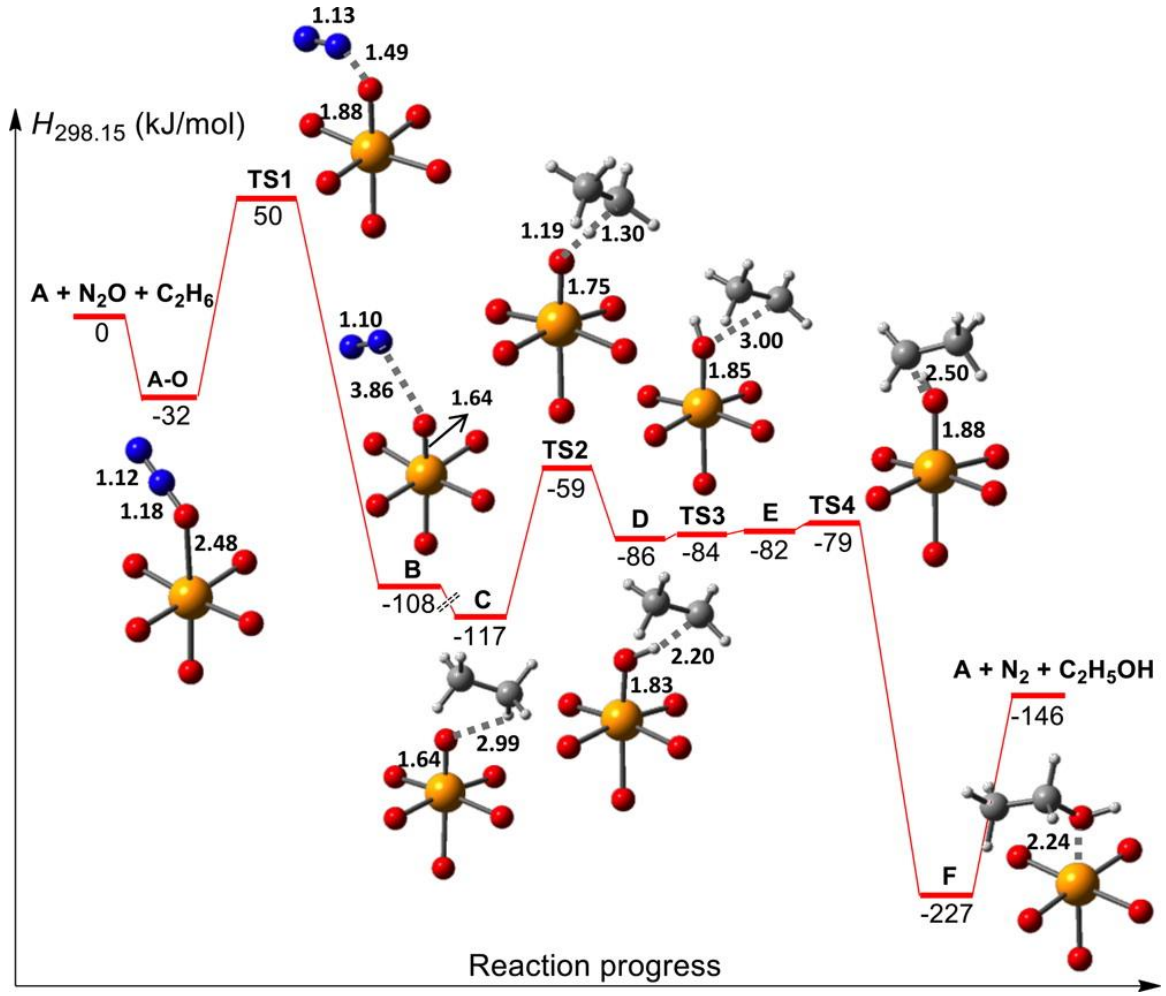

Figure 9: Enthalpy profile of ethane to ethanol catalytic cycle calculated using M06-L on an 88-atom cluster. Reprinted with permission from Ref. [242]. Copyright 2015, American Chemical Society.

Methane and ethane activation were also studied by Vitillo et al.[245] In that work, a cluster model representing a metal node similar to what could be found in MOFs such as MIL-100 and MIL101. The cluster featured three metal sites, one of which was held constant as Fe while the other two could be Al, Cr, or Fe (**Figure 10**). Most work was conducted with DFT using the M06-L[125] functional, but CASSCF/CASPT2 were also performed on the **A** structure in **Figure 10** for the FeFeFe clusters and the AlAlFe cases, with (16,15) and (6,5) active spaces, respectively. These were seen as minimal active spaces (featuring only the 3*d* orbitals of the Fe), but the choices was justified by showing that the energies of relative spin states in the AlAlFe

cluster did not change significantly with larger active spaces. Both M06-L and CASPT2 predicted high-spin on all Fe and Cr centers, but the degree of difference was not consistent across methods: M06-L calculated the triplet-quintet splitting for the Fe center in AlAlFe to be 100 kJ/mol in favor of the quintet, while the CASPT2 results indicated the quintet would be favored by over 180 kJ/mol. The primary use of the CASPT2 calculations was to justify performing the DFT reaction coordinate calculations on the high-spin surfaces. Other than AlAlFe the clusters studied were found to have an overall intermediate spin due to antiferromagnetic coupling of the individually high-spin centers, but CASPT2 results from FeFeFe demonstrated that the high-spin state was less than 22 kJ/mol above ground, demonstrating that the coupling between the high-spin centers was sufficiently weak for it to be ignored for subsequent calculations. CASPT2 was also able to correctly identify that there would be two Fe(III) and one Fe(II) centers in the FeFeFe cluster, in agreement with past experiment, while DFT incorrectly predicted all three Fe centers would be in equivalent intermediate oxidation states.

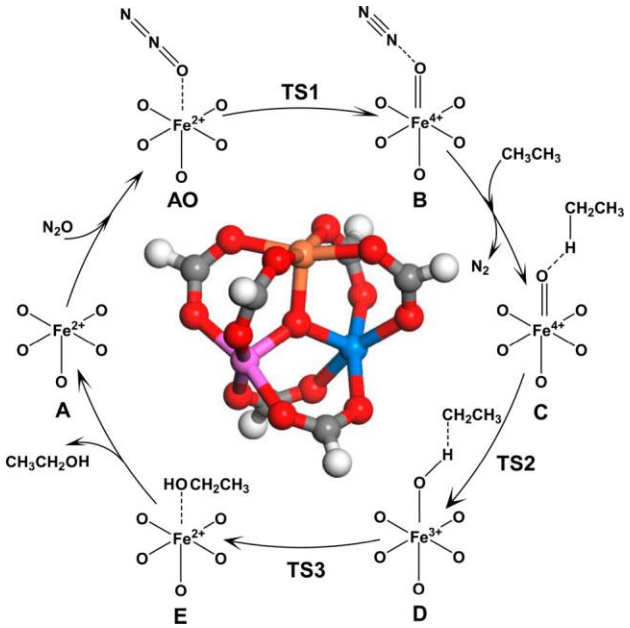

Figure 10: Model cluster $M_1(III)M_2(III)Fe(II)(\mu_3\text{-}O)(HCOO)_6$, where M_1 and M_2 can be Al, Cr, or Fe. Shown here with ethane to ethanol catalytic cycle. Reprinted with permission from Ref. [245]. Copyright 2018, American Chemical Society.

Bernales et al.[246,247] analyzed the mechanisms of ethylene dimerization using cobalt or nickel (deposited on the NU-1000 MOF) using DFT and found nickel to have a lower activation barrier than cobalt. CASPT2 calculations were performed in order to rationalize the different reactivity between Co and Ni. The active spaces included two C 2*p* orbitals from the π bonds of the ethylene and five and four of the Co and Ni 3*d* orbitals, along with the corresponding 3*d′* "second-shell" orbitals. Ni had a smaller active space due to it being low-spin in a square-planar conformation, which led to one of the 3*d* orbitals being unoccupied. Differences in the degree of involvement of the 3d orbitals of the metal in the transition state proved to be the driving force in the differences in Co and Ni reactivity: For the Ni case, a single formally empty *d* orbital interacts strongly (48%) with the 2*p* orbitals of the ethylene carbon atoms (52%). For Co the equivalent *d* orbital is singly occupied, leading to a partially occupied antibonding configuration and only a 15% 3*d* orbital contribution in the frontier molecular orbital. Even though MR calculations were not used for computing reaction (or activation) energies, this example shows how MR methods can be useful in understanding reactivity in catalysis.

Finally, an example a full catalytic pathway calculated with MR methods is the study by Chalupský et al.[248] of C-C desaturation through C-H activation by Δ^9 desaturase, an enzyme with two Fe atoms at the active site that can perform dehydrogenation on alkyl chains (**Figure 11**). Although it is not, strictly speaking, a heterogeneous catalytic reaction, we include it as one of the rare examples of a multireference approach applied to a catalytic reaction pathway, demonstrating many of the benefits and challenges involved. The authors analyzed different reaction pathways employing DMRG/CASPT2 with active spaces including all 3*d* orbitals on Fe, all 2*s* and 2*p* O_2 orbitals, C−H σ and σ* orbitals of the substrate. When a water molecule was present, all of its valence orbitals were included as well. The authors argue that because of the size of their active spaces (between (20,20) and (35,26)) they can assume their DMRG calculations provide the correct qualitative description of the reaction pathway. Selecting the lowest-energy results for each intermediate and transition state led them to suggest proton-

assisted O_2 activation as the mechanism for C-C desaturation. They then compared their DMRG/CASPT2 activation and reaction energies with DFT results employing most popular functionals. They observed large variances among the DFT results, with mean absolute deviations from the DMRG/CASPT2 values in the tens of kJ/mol for all functionals and with maximum deviations usually in excess of 70 kJ/mol. Moreover, they note that several of the DFT functionals predict qualitatively incorrect reaction pathways leading to hydroxylation rather than the experimentally observed desaturation.

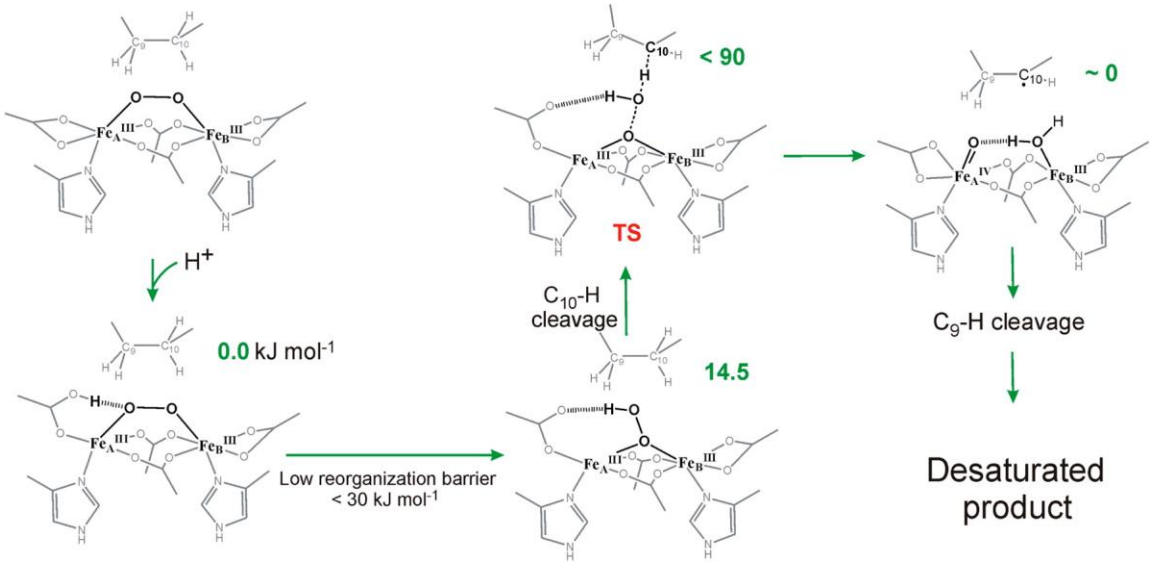

Figure 11: Mechanism of Δ^9 desaturase predicted by DMRG-CASPT2. Reprinted with permission from Ref. [248]. Copyright 2014, American Chemical Society.

Before we conclude this section, it is worth mentioning that when a cluster model of a periodic system is used (whether for DFT or MR wave function theory), the choice of the cluster is very important. For example, in MOF-based catalysis it is common to use a cluster model to analyze the catalytic mechanisms when the catalysis occurs at well-separated single-sites within only one node. The challenge arises in deciding where to cut the linkers connecting two nodes. For example, BDC (benzene-1,4-dicarboxylic acid) linkers can be replaced by benzoate, formate or acetate linkers to have a finite cluster. Additionally, in order to mimic the rigidity of the

framework some of the linker atoms have to be frozen at the geometry of the optimized periodic structure (which takes into account the rigidity of the overall structure), although in principle this freezing could also introduce artifacts. Simons et al.[147] replaced the structural linkers of NU-1000 with acetate ligands and froze the cooordinates of the atoms constituting the methyl groups. In their work on ethylene dimerization on NU-1000,[246] Bernales et al. replaced the structural linkers with formate ligands for their mechanistic study (which reduced the computational cost) and the carbon atoms of the formate groups were frozen during optimization. Studies of UiO-66 and -67 for ethanol dehydration by Yang et al.[249] featured replacing BDC linkers with 4 benzoate and 7 formate groups (leaving 1 defect site), and only the p-carbon atoms of the benzoate linkers were fixed during optimization in order to mimic the MOF rigidity. Interested readers can also consult Ref. [242] and references therein, which address the selection and validation of an 88-atom cluster representing a MOF-74 node for DFT calculations and a smaller 26-atom cluster for CASPT2.

6. Outlook

Heterogeneous catalysis is in widespread use for chemical transformations and is of fundamental importance in industry. Over the years, DFT has proven to be an invaluable tool and remains a popular method for the computational modeling of catalysis, with still relatively few applications of MR wave function theory methods to corresponding problems owing to the greater efficiency of the DFT model. However, the common presence of transition metals in catalysis generates challenges for DFT because corresponding MR character (either in the ground electronic state, thermally accessible excited states, or both) makes it difficult to accurately describe the energetics of different spin states, spin density distributions (in open-shell systems), and oxidation states. Examples from the literature include cases where, in multi metallic systems, one functional will assign spin density to one metal while another functional will assign it to the other.[105] Moreover, in view of the increasing use of machine learning for catalysis, it is imperative that the input (training) data be very accurate in order to try to avoid biased and chemically meaningless predictions.

The very few available MR studies on catalytic mechanisms already show that there can be dramatic differences between DFT and MR methods. However, MR methods have their own drawbacks, both for catalysis and reactivity in general, because reliable results require a balanced active space along the entire reaction path and this is not always practical. This is the main reason that active-space based methods have been used more for spectroscopy than for reactivity, even if there are examples of the latter.

The general challenges of MR methodologies are that they are very expensive and they are not as “black-box” as DFT. A careful selection of the active space is absolutely crucial, as well as a careful inspection of the outcome of the calculation. Large active spaces may be needed in order to get accurate results when there are various parts of the system under consideration that are strongly correlated, in which case calculations can become prohibitively expensive. The high computational cost and the need for specialized expertise have slowed the mainstream use

of MR theories in computational heterogeneous (and homogeneous) catalysis. However, work towards reducing the cost of the calculations and automatizing the active space choice is ongoing. Examples for reducing the cost include the development of the RASSCF and GASSCF models,[170] which use fewer CSFs than CASSCF, and MC-PDFT,[110,203] which can account for dynamical correlation at much lower cost compared to CASPT2.

Another problem with these methods is that even when they can be used relatively efficiently to obtain single-point energies, geometry optimizations remain more challenging and less black box, especially with CASPT2, so the standard procedure is to generate potential energy surfaces with KS-DFT and then compute single-point energies with these more advanced methods, which can obviously be problematic when the KS-DFT model is so qualitatively inaccurate that the potential energy surface becomes suspect. Recent analytical gradient implementations for MC-PDFT may enable accurate geometry optimizations at this particular MR level.[193,194,250] Regarding automatizing active space choice, work has begun to appear in the literature.[181,183]

An important point meriting consideration is that common practice is to follow a reaction along a single spin-state potential energy surface, but catalysis can include reactions exhibiting two-state reactivity. Spin-orbit coupling may moreover be important for such cases.[251–254] We note the potential importance of MR methods for modeling spin forbidden reactions that may involve MR character (especially in lower spin states, owing to the higher number of possible determinants or CSFs for such states). Two state reactivity has been repeatedly invoked in metal-based reactions,[255–258] and MR methods can offer important insights into such processes.

Heterogeneous catalysis typically implies use of solid-state catalysts, and since heterogeneous catalysis usually is modeled using periodic calculations, it is unsurprising that no literature associated with the use of MR methods has yet appeared, although often it is proven possible to extract valuable information from a realistic cluster model. In this regard, catalysis on metal or metal oxide surfaces (e.g., for electrocatalytic applications) are expected to encounter

the same problems as molecular systems. There is no particular reason that prevents the drawbacks of DFT found in a molecular complex from being extended to periodic systems. Furthermore, there are problems associated with DFT band gap[259–261] and bandstructure[262–264] predictions for strongly correlated systems, which are relevant issues for photocatalysis. Work toward implementation of CASSCF in periodic systems using density matrix embedding theory (DMET)[265,266] is underway, and other progress has also been made in this direction.[267–274]

In summary, while DFT remains a generally robust first choice for modeling catalytic reactions, we believe that the field has advanced sufficiently that the computational modeling of catalysis should more regularly move a step forward and go beyond DFT to consider the use of more flexible wave-function electronic structure theories, including MR methods. Continued development to address the current practical challenges associated with the use of MR methods is certain to foster their increased usage.

AUTHOR INFORMATION

Corresponding Author

*L. G. E-mail: gagliard@umn.edu

ORCID

Carlo Alberto Gaggioli: 0000-0001-9105-8731

Samuel J. Stoneburner: 0000-0001-8394-0572

Christopher J. Cramer: 0000-0001-5048-1859

Laura Gagliardi: 0000-0001-5227-1396

Notes

The authors declare no competing financial interest.

ACKNOWLEDGEMENTS

This work was supported by the Inorganometallic Catalyst Design Center, an EFRC funded by the DOE, Office of Basic Energy Sciences (DE-SC0012702).

References:

(1) Medford, A. J.; Vojvodic, A.; Hummelshøj, J. S.; Voss, J.; Abild-Pedersen, F.; Studt, F.; Bligaard, T.; Nilsson, A.; Nørskov, J. K. From the Sabatier Principle to a Predictive Theory of Transition-Metal Heterogeneous Catalysis. *J. Catal.* **2015**, *328*, 36–42.

(2) Schlögl, R. Heterogeneous Catalysis. *Angew. Chemie - Int. Ed.* **2015**, *54*, 3465–3520.

(3) Lian, T.; Koper, M. T. M.; Reuter, K.; Subotnik, J. E. Special Topic on Interfacial Electrochemistry and Photo(Electro)Catalysis. *J. Chem. Phys.* **2019**, *150*, 041401.

(4) Horn, R.; Schlögl, R. Methane Activation by Heterogeneous Catalysis. *Catal. Letters* **2015**, *145*, 23–39.

(5) Sauer, J.; Freund, H. J. Models in Catalysis. *Catal. Letters* **2015**, *145*, 109–125.

(6) Olivos-Suarez, A. I.; Szécsényi, À.; Hensen, E. J. M.; Ruiz-Martinez, J.; Pidko, E. A.; Gascon, J. Strategies for the Direct Catalytic Valorization of Methane Using Heterogeneous Catalysis: Challenges and Opportunities. *ACS Catal.* **2016**, *6*, 2965–2981.

(7) Latimer, A. A.; Kulkarni, A. R.; Aljama, H.; Montoya, J. H.; Yoo, J. S.; Tsai, C.; Abild-Pedersen, F.; Studt, F.; Nørskov, J. K. Understanding Trends in C-H Bond Activation in Heterogeneous Catalysis. *Nat. Mater.* **2017**, *16*, 225–229.

(8) Mahyuddin, M. H.; Shiota, Y.; Staykov, A.; Yoshizawa, K. Theoretical Overview of Methane Hydroxylation by Copper-Oxygen Species in Enzymatic and Zeolitic Catalysts. *Acc. Chem. Res.* **2018**, *51*, 2382–2390.

(9) Lesthaeghe, D.; Van Speybroeck, V.; Marin, G. B.; Waroquier, M. Understanding the Failure of Direct C-C Coupling in the Zeolite-Catalyzed Methanol-to-Olefin Process. *Angew. Chemie - Int. Ed.* **2006**, *118*, 1746 –1751.

(10) McCann, D. M.; Lesthaeghe, D.; Kletnieks, P. W.; Guenther, D. R.; Hayman, M. J.; Van Speybroeck, V.; Waroquier, M.; Haw, J. F. A Complete Catalytic Cycle for Supramolecular Methanol-to-Olefins Conversion by Linking Theory with Experiment. *Angew. Chemie - Int. Ed.* **2008**, *120*, 5257 –5260.

(11) Quaino, P.; Juarez, F.; Santos, E.; Schmickler, W. Volcano Plots in Hydrogen Electrocatalysis-Uses and Abuses. *Beilstein J. Nanotechnol.* **2014**, *5*, 846–854.

(12) Brodsky, C. N.; Hadt, R. G.; Hayes, D.; Reinhart, B. J.; Li, N.; Chen, L. X.; Nocera, D. G. In Situ Characterization of Cofacial Co(IV) Centers in Co_4O_4 Cubane: Modeling the High-Valent Active Site in Oxygen-Evolving Catalysts. *Proc. Natl. Acad. Sci.* **2017**, *114* (15), 3855–3860.

(13) Chen, P.; Zhou, T.; Xing, L.; Xu, K.; Tong, Y.; Xie, H.; Zhang, L.; Yan, W.; Chu, W.; Wu, C.; et al. Atomically Dispersed Iron–Nitrogen Species as Electrocatalysts for Bifunctional Oxygen Evolution and Reduction Reactions. *Angew. Chemie - Int. Ed.* **2017**, *56*, 610–614.

(14) Reier, T.; Nong, H. N.; Teschner, D.; Schlögl, R.; Strasser, P. Electrocatalytic Oxygen Evolution Reaction in Acidic Environments - Reaction Mechanisms and Catalysts. *Adv. Energy Mater.* **2017**, *7*, 1601275.

(15) Suen, N. T.; Hung, S. F.; Quan, Q.; Zhang, N.; Xu, Y. J.; Chen, H. M. Electrocatalysis for the Oxygen Evolution Reaction: Recent Development and Future Perspectives. *Chem. Soc. Rev.* **2017**, *46*, 337–365.

(16) Plaisance, C. P.; Beinlich, S. D.; Reuter, K. Kinetics-Based Computational Catalyst Design Strategy for the Oxygen Evolution Reaction on Transition-Metal Oxide Surfaces. *J. Phys. Chem. C* **2018**, [Online early access]. DOI: 10.1021/acs.jpcc.8b085.

(17) Li, Y.; Chan, S. H.; Sun, Q. Heterogeneous Catalytic Conversion of CO_2: A Comprehensive Theoretical Review. *Nanoscale* **2015**, *7*, 8663–8683.
(18) Lessio, M.; Senftle, T. P.; Carter, E. A. Is the Surface Playing a Role during Pyridine-Catalyzed CO_2 Reduction on p-GaP Photoelectrodes? *ACS Energy Lett.* **2016**, *1*, 464–468.
(19) Yoo, J. S.; Christensen, R.; Vegge, T.; Nørskov, J. K.; Studt, F. Theoretical Insight into the Trends That Guide the Electrochemical Reduction of Carbon Dioxide to Formic Acid. *ChemSusChem* **2016**, *9*, 358–363.
(20) Lessio, M.; Dieterich, J. M.; Carter, E. A. Hydride Transfer at the GaP(110)/Solution Interface: Mechanistic Implications for CO_2 Reduction Catalyzed by Pyridine. *J. Phys. Chem. C* **2017**, *121*, 17321–17331.
(21) Garza, A. J.; Bell, A. T.; Head-Gordon, M. Is Subsurface Oxygen Necessary for the Electrochemical Reduction of CO_2 on Copper? *J. Phys. Chem. Lett.* **2018**, *9*, 601–606.
(22) Garza, A. J.; Bell, A. T.; Head-Gordon, M. Mechanism of CO_2 Reduction at Copper Surfaces: Pathways to C_2 Products. *ACS Catal.* **2018**, *8*, 1490–1499.
(23) Lee, A. F.; Bennett, J. A.; Manayil, J. C.; Wilson, K. Heterogeneous Catalysis for Sustainable Biodiesel Production via Esterification and Transesterification. *Chem. Soc. Rev.* **2014**, *43*, 7887–7916.
(24) Rajan, K. Combinatorial Materials Sciences: Experimental Strategies for Accelerated Knowledge Discovery. *Annu. Rev. Mater. Res.* **2008**, *38*, 299–322.
(25) Tong, L.; Thummel, R. P. Mononuclear Ruthenium Polypyridine Complexes That Catalyze Water Oxidation. *Chem. Sci.* **2016**, *7*, 6591–6603.
(26) Costentin, C.; Robert, M.; Savéant, J.-M. Current Issues in Molecular Catalysis Illustrated by Iron Porphyrins as Catalysts of the CO_2-to-CO Electrochemical Conversion. *Acc. Chem. Res.* **2015**, *48*, 2996–3006.
(27) Gascon, J.; Aktay, U.; Hernandez-Alonso, M. D.; van Klink, G. P. M.; Kapteijn, F. Amino-Based Metal-Organic Frameworks as Stable, Highly Active Basic Catalysts. *J. Catal.* **2009**, *261*, 75–87.
(28) Stephen, A.; Hashmi, K. Homogeneous Gold Catalysis beyond Assumptions and Proposals-Characterized Intermediates. *Angew. Chemie - Int. Ed.* **2010**, *49*, 5232–5241.
(29) Hemelsoet, K.; Van Der Mynsbrugge, J.; De Wispelaere, K.; Waroquier, M.; Van Speybroeck, V. Unraveling the Reaction Mechanisms Governing Methanol-to-Olefins Catalysis by Theory and Experiment. *ChemPhysChem* **2013**, *14*, 1526–1545.
(30) Nørskov, J. K.; Bligaard, T.; Rossmeisl, J.; Christensen, C. H. Towards the Computational Design of Solid Catalysts. *Nat. Chem.* **2009**, *1*, 37–46.
(31) Thiel, W. Computational Catalysis - Past, Present, and Future. *Angew. Chemie - Int. Ed.* **2014**, *53*, 8605–8613.
(32) Kohn, W.; Sham, L. J. Self-Consistent Equations Including Exchange and Correlation Effects. *Phys. Rev.* **1965**, *140* (4A), A1133–A1138.
(33) Abild-Pedersen, F.; Greeley, J.; Studt, F.; Rossmeisl, J.; Munter, T. R.; Moses, P. G.; Skúlason, E.; Bligaard, T.; Nørskov, J. K. Scaling Properties of Adsorption Energies for Hydrogen-Containing Molecules on Transition-Metal Surfaces. *Phys. Rev. Lett.* **2007**, *99*, 016105.
(34) Greeley, J. Theoretical Heterogeneous Catalysis: Scaling Relationships and Computational Catalyst Design. *Annu. Rev. Chem. Biomol. Eng.* **2016**, *7*, 605–635.
(35) Yarulina, I.; De Wispelaere, K.; Bailleul, S.; Goetze, J.; Radersma, M.; Abou-Hamad, E.; Vollmer, I.; Goesten, M.; Mezari, B.; Hensen, E. J. M.; et al. Structure–Performance

Descriptors and the Role of Lewis Acidity in the Methanol-to-Propylene Process. *Nat. Chem.* **2018**, *10*, 804–812.
(36) Sabatier, P. *La Catalyse En Chimie Organique*; Berauge: Paris, 1920.
(37) Falivene, L.; Kozlov, S. M.; Cavallo, L. Constructing Bridges between Computational Tools in Heterogeneous and Homogeneous Catalysis. *ACS Catal.* **2018**, *8*, 5637–5656.
(38) Busch, M.; Fabrizio, A.; Luber, S.; Hutter, J.; Corminboeuf, C. Exploring the Limitation of Molecular Water Oxidation Catalysts. *J. Phys. Chem. C* **2018**, *122*, 12404–12412.
(39) Wodrich, M. D.; Sawatlon, B.; Busch, M.; Corminboeuf, C. On the Generality of Molecular Volcano Plots. *ChemCatChem* **2018**, *10*, 1586–1591.
(40) Yan, J.; Gorai, P.; Ortiz, B.; Miller, S.; Barnett, S. A.; Mason, T.; Stevanović, V.; Toberer, E. S. Material Descriptors for Predicting Thermoelectric Performance. *Energy Environ. Sci.* **2015**, *8*, 983–994.
(41) Jain, A.; Shin, Y.; Persson, K. A. Computational Predictions of Energy Materials Using Density Functional Theory. *Nat. Rev. Mater.* **2016**, *1*, 1–13.
(42) James, S. L. Metal-Organic Frameworks. *Chem. Soc. Rev.* **2003**, *32*, 276–288.
(43) Long, J. R.; Yaghi, O. M. The Pervasive Chemistry of Metal–Organic Frameworks. *Chem. Soc. Rev.* **2009**, *38*, 1213–1214.
(44) Zhou, H.-C.; Long, J. R.; Yaghi, O. M. Introduction to Metal–Organic Frameworks. *Chem. Rev.* **2012**, *112*, 673–674.
(45) Furukawa, H.; Cordova, K. E.; O'Keeffe, M.; Yaghi, O. M. The Chemistry and Applications of Metal-Organic Frameworks. *Science.* **2013**, *341*, 1230444.
(46) Mlinar, A. N.; Keitz, B. K.; Gygi, D.; Bloch, E. D.; Long, J. R.; Bell, A. T. Selective Propene Oligomerization with Nickel(II)-Based Metal-Organic Frameworks. *ACS Catal.* **2014**, *4*, 717–721.
(47) Nguyen, H. G. T.; Schweitzer, N. M.; Chang, C. Y.; Drake, T. L.; So, M. C.; Stair, P. C.; Farha, O. K.; Hupp, J. T.; Nguyen, S. T. Vanadium-Node-Functionalized UiO-66: A Thermally Stable MOF-Supported Catalyst for the Gas-Phase Oxidative Dehydrogenation of Cyclohexene. *ACS Catal.* **2014**, *4*, 2496–2500.
(48) García-García, P.; Müller, M.; Corma, A. MOF Catalysis in Relation to Their Homogeneous Counterparts and Conventional Solid Catalysts. *Chem. Sci.* **2014**, *5*, 2979–3007.
(49) Zhao, M.; Ou, S.; Wu, C. De. Porous Metal-Organic Frameworks for Heterogeneous Biomimetic Catalysis. *Acc. Chem. Res.* **2014**, *47*, 1199–1207.
(50) Hod, I.; Sampson, M. D.; Deria, P.; Kubiak, C. P.; Farha, O. K.; Hupp, J. T. Fe-Porphyrin-Based Metal-Organic Framework Films as High-Surface Concentration, Heterogeneous Catalysts for Electrochemical Reduction of CO_2. *ACS Catal.* **2015**, *5*, 6302–6309.
(51) Meyer, K.; Ranocchiari, M.; Van Bokhoven, J. A. Metal Organic Frameworks for Photo-Catalytic Water Splitting. *Energy Environ. Sci.* **2015**, *8*, 1923–1937.
(52) Doonan, C. J.; Sumby, C. J. Metal-Organic Framework Catalysis. *CrystEngComm* **2017**, *19*, 4045–4049.
(53) Rogge, S. M. J.; Bavykina, A.; Hajek, J.; Garcia, H.; Olivos-Suarez, A. I.; Sepúlveda-Escribano, A.; Vimont, A.; Clet, G.; Bazin, P.; Kapteijn, F.; et al. Metal-Organic and Covalent Organic Frameworks as Single-Site Catalysts. *Chem. Soc. Rev.* **2017**, *46*, 3134–3184.
(54) Wu, C.-D.; Zhao, M. Incorporation of Molecular Catalysts in Metal–Organic Frameworks for Highly Efficient Heterogeneous Catalysis. *Adv. Mater.* **2017**, *29*, 1605446.

(55) Zhu, L.; Liu, X. Q.; Jiang, H. L.; Sun, L. B. Metal-Organic Frameworks for Heterogeneous Basic Catalysis. *Chem. Rev.* **2017**, *117*, 8129–8176.
(56) Lee, J.; Farha, O. K.; Roberts, J.; Scheidt, K. A.; Nguyen, S. T.; Hupp, J. T. Metal-Organic Framework Materials as Catalysts. *Chem. Soc. Rev.* **2009**, *38*, 1450–1459.
(57) Odoh, S. O.; Cramer, C. J.; Truhlar, D. G.; Gagliardi, L. Quantum-Chemical Characterization of the Properties and Reactivities of Metal–Organic Frameworks. *Chem. Rev.* **2015**, *115*, 6051–6111.
(58) Doitomi, K.; Hirao, H. Hybrid Computational Approaches for Deriving Quantum Mechanical Insights into Metal–Organic Frameworks. *Tetrahedron Lett.* **2017**, *58*, 2309–2317.
(59) Bernales, V.; Ortuño, M. A.; Truhlar, D. G.; Cramer, C. J.; Gagliardi, L. Computational Design of Functionalized Metal-Organic Framework Nodes for Catalysis. *ACS Cent. Sci.* **2018**, *4*, 5–19.
(60) Laidler, K. J.; King, M. C. The Development of Transition-State Theory. *J. Phys. Chem.* **1983**, *87*, 2657–2664.
(61) Truhlar, D. G.; Garrett, B. C.; Klippenstein, S. J. Current Status of Transition-State Theory. *J. Phys. Chem.* **1996**, *100*, 12771–12800.
(62) Bligaard, T.; Nørskov, J. K.; Dahl, S.; Matthiesen, J.; Christensen, C. H.; Sehested, J. The Brønsted-Evans-Polanyi Relation and the Volcano Curve in Heterogeneous Catalysis. *J. Catal.* **2004**, *224*, 206–217.
(63) Jørgensen, M.; Grönbeck, H. First-Principles Microkinetic Modeling of Methane Oxidation over Pd(100) and Pd(111). *ACS Catal.* **2016**, *6*, 6730–6738.
(64) Mao, Y.; Wang, H.-F.; Hu, P. Theory and Applications of Surface Micro-Kinetics in the Rational Design of Catalysts Using Density Functional Theory Calculations. *Wiley Interdiscip. Rev. Comput. Mol. Sci.* **2017**, *7*, e1321.
(65) Van Speybroeck, V.; De Wispelaere, K.; Van der Mynsbrugge, J.; Vandichel, M.; Hemelsoet, K.; Waroquier, M. First Principle Chemical Kinetics in Zeolites: The Methanol-to-Olefin Process as a Case Study. *Chem. Soc. Rev.* **2014**, *43*, 7326–7357.
(66) Catlow, C. R. A.; Waroquier, M.; Bell, R. G.; Hemelsoet, K.; Van Speybroeck, V.; Joos, L. Advances in Theory and Their Application within the Field of Zeolite Chemistry. *Chem. Soc. Rev.* **2015**, *44* (20), 7044–7111.
(67) Cnudde, P.; De Wispelaere, K.; Vanduyfhuys, L.; Demuynck, R.; Van Der Mynsbrugge, J.; Waroquier, M.; Van Speybroeck, V. How Chain Length and Branching Influence the Alkene Cracking Reactivity on H-ZSM-5. *ACS Catal.* **2018**, *8*, 9579–9595.
(68) Van Speybroeck, V.; Head-Gordon, M.; Bell, A. T.; Van der Mynsbrugge, J.; Lin, L.-C. C.; Janda, A.; Lin, L.-C. C.; Van Speybroeck, V.; Head-Gordon, M.; Bell, A. T. Understanding Brønsted-Acid Catalyzed Monomolecular Reactions of Alkanes in Zeolite Pores by Combining Insights from Experiment and Theory. *ChemPhysChem* **2018**, *19*, 341–358.
(69) Janet, J. P.; Kulik, H. J. Predicting Electronic Structure Properties of Transition Metal Complexes with Neural Networks. *Chem. Sci.* **2017**, *8*, 5137–5152.
(70) Janet, J. P.; Kulik, H. J. Resolving Transition Metal Chemical Space: Feature Selection for Machine Learning and Structure-Property Relationships. *J. Phys. Chem. A* **2017**, *121*, 8939–8954.
(71) Ulissi, Z. W.; Medford, A. J.; Bligaard, T.; Nørskov, J. K. To Address Surface Reaction Network Complexity Using Scaling Relations Machine Learning and DFT Calculations.

Nat. Commun. **2017**, *8*, 1–7.
(72) Ulissi, Z. W.; Tang, M. T.; Xiao, J.; Liu, X.; Torelli, D. A.; Karamad, M.; Cummins, K.; Hahn, C.; Lewis, N. S.; Jaramillo, T. F.; et al. Machine-Learning Methods Enable Exhaustive Searches for Active Bimetallic Facets and Reveal Active Site Motifs for CO_2 Reduction. *ACS Catal.* **2017**, *7*, 6600–6608.
(73) Janet, J. P.; Chan, L.; Kulik, H. J. Accelerating Chemical Discovery with Machine Learning: Simulated Evolution of Spin Crossover Complexes with an Artificial Neural Network. *J. Phys. Chem. Lett.* **2018**, *9*, 1064–1071.
(74) Margraf, J. T.; Reuter, K. Making the Coupled Cluster Correlation Energy Machine-Learnable. *J. Phys. Chem. A* **2018**, *122*, 6343–6348.
(75) Meyer, B.; Sawatlon, B.; Heinen, S.; Von Lilienfeld, O. A.; Corminboeuf, C. Machine Learning Meets Volcano Plots: Computational Discovery of Cross-Coupling Catalysts. *Chem. Sci.* **2018**, *9*, 7069–7077.
(76) Nandy, A.; Duan, C.; Janet, J. P.; Gugler, S.; Kulik, H. J. Strategies and Software for Machine Learning Accelerated Discovery in Transition Metal Chemistry. *Ind. Eng. Chem. Res.* **2018**, *57*, 13973–13986.
(77) Grisafi, A.; Fabrizio, A.; Meyer, B.; Wilkins, D. M.; Corminboeuf, C.; Ceriotti, M. Transferable Machine-Learning Model of the Electron Density. *ACS Cent. Sci.* **2019**, *5*, 57–64.
(78) Janet, J. P.; Liu, F.; Nandy, A.; Duan, C.; Yang, T.; Lin, S.; Kulik, H. J. Designing in the Face of Uncertainty: Exploiting Electronic Structure and Machine Learning Models for Discovery in Inorganic Chemistry. *Inorg. Chem.* **2019**, [Online early access]. DOI: 10.1021/9b00109.
(79) Goldsmith, B. R.; Esterhuizen, J.; Liu, J.-X.; Bartel, C. J.; Sutton, C. Machine Learning for Heterogeneous Catalyst Design and Discovery. *AIChE J.* **2018**, *64* (7), 2311–2323.
(80) Shapeev, A. V. Moment Tensor Potentials: A Class of Systematically Improvable Interatomic Potentials. *Multiscale Model. Simul.* **2016**, *14* (3), 1153–1173.
(81) Boes, J. R.; Kitchin, J. R. Neural Network Predictions of Oxygen Interactions on a Dynamic Pd Surface. *Mol. Simul.* **2017**, *43* (5–6), 346–354.
(82) Zhai, H.; Alexandrova, A. N. Fluxionality of Catalytic Clusters: When It Matters and How to Address It. *ACS Catal.* **2017**, *7*, 1905–1911.
(83) Torelli, D. A.; Francis, S. A.; Crompton, J. C.; Javier, A.; Thompson, J. R.; Brunschwig, B. S.; Soriaga, M. P.; Lewis, N. S. Nickel-Gallium-Catalyzed Electrochemical Reduction of CO_2 to Highly Reduced Products at Low Overpotentials. *ACS Catal.* **2016**, *6*, 2100–2104.
(84) Saravanan, K.; Kitchin, J. R.; Von Lilienfeld, O. A.; Keith, J. A. Alchemical Predictions for Computational Catalysis: Potential and Limitations. *J. Phys. Chem. Lett.* **2017**, *8*, 5002–5007.
(85) Piccini, G.; Alessio, M.; Sauer, J. Ab-Initio Calculation of Rate Constants for Molecule-Surface Reactions with Chemical Accuracy. *Angew. Chemie - Int. Ed.* **2016**, *55*, 5235–5237.
(86) Alessio, M.; Bischoff, F. A.; Sauer, J. Chemically Accurate Adsorption Energies for Methane and Ethane Monolayers on the MgO(001) Surface. *Phys. Chem. Chem. Phys.* **2018**, *20*, 9760–9769.
(87) Piccini, G.; Alessio, M.; Sauer, J. Ab Initio Study of Methanol and Ethanol Adsorption on Brønsted Sites in Zeolite H-MFI. *Phys. Chem. Chem. Phys.* **2018**, *20*, 19664–19670.

(88) Lejaeghere, K.; Van Speybroeck, V.; Van Oost, G.; Cottenier, S. Error Estimates for Solid-State Density-Functional Theory Predictions: An Overview by Means of the Ground-State Elemental Crystals. *Crit. Rev. Solid State Mater. Sci.* **2014**, *39*, 1–24.
(89) Jacob, C. R.; Reiher, M. Spin in Density-Functional Theory. *Int. J. Quantum Chem.* **2012**, *112*, 3661–3684.
(90) Yu, H. S.; Li, S. L.; Truhlar, D. G. Perspective: Kohn-Sham Density Functional Theory Descending a Staircase. *J. Chem. Phys.* **2016**, *145*, 130901.
(91) Jiang, W.; Deyonker, N. J.; Wilson, A. K. Multireference Character for 3d Transition-Metal-Containing Molecules. *J. Chem. Theory Comput.* **2012**, *8*, 460–468.
(92) Wang, J.; Manivasagam, S.; Wilson, A. K. Multireference Character for 4d Transition Metal-Containing Molecules. *J. Chem. Theory Comput.* **2015**, *11*, 5865–5872.
(93) Perdew, J. P.; Parr, R. G.; Levy, M.; Balduz Jr, J. L. Density-Functional Theory for Fractional Particle Number: Derivative Discontinuities of the Energy. *PRL* **1982**, *49* (23), 1691–1694.
(94) Yang, W.; Zhang, Y.; Ayers, P. W. Degenerate Ground States and a Fractional Number of Electrons in Density and Reduced Density Matrix Functional Theory. *Phys. Rev. Lett.* **2000**, *84* (22), 5172–5175.
(95) Zhang, Y.; Yang, W. Perspective on "Density-Functional Theory for Fractional Particle Number: Derivative Discontinuities of the Energy." *Theor. Chem. Acc.* **2000**, *103*, 346–348.
(96) Mori-Sánchez, P.; Cohen, A. J.; Yang, W. Many-Electron Self-Interaction Error in Approximate Density Functionals. *J. Chem. Phys.* **2006**, *125*, 201102.
(97) Ruzsinszky, A.; Perdew, J. P.; Csonka, G. I.; Vydrov, O. A.; Scuseria, G. E. Density Functionals That Are One- and Two- Are Not Always Many-Electron Self-Interaction-Free, as Shown for H_2^+ He_2^+, Li H^+, and Ne_2^+. *J. Chem. Phys.* **2007**, *126*, 104102.
(98) Haunschild, R.; Henderson, T. M.; Jiménez-Hoyos, C. A.; Scuseria, G. E. Many-Electron Self-Interaction and Spin Polarization Errors in Local Hybrid Density Functionals. *J. Chem. Phys.* **2010**, *133*, 134116.
(99) Cohen, A. J.; Mori-Sánchez, P.; Yang, W. Challenges for Density Functional Theory. *Chem. Rev.* **2012**, *112*, 289–320.
(100) Kim, M. C.; Sim, E.; Burke, K. Understanding and Reducing Errors in Density Functional Calculations. *Phys. Rev. Lett.* **2013**, *111*, 073003.
(101) Schmidt, T.; Kümmel, S. One- and Many-Electron Self-Interaction Error in Local and Global Hybrid Functionals. *Phys. Rev. B* **2016**, *93*, 165120.
(102) Mori-Sánchez, P.; Cohen, A. J.; Yang, W. Localization and Delocalization Errors in Density Functional Theory and Implications for Band-Gap Prediction. *Phys. Rev. Lett.* **2008**, *100*, 146401.
(103) Zheng, X.; Liu, M.; Johnson, E. R.; Contreras-García, J.; Yang, W. Delocalization Error of Density-Functional Approximations: A Distinct Manifestation in Hydrogen Molecular Chains. *J. Chem. Phys.* **2012**, *137*, 214106.
(104) Johnson, E. R.; Otero-De-La-Roza, A.; Dale, S. G. Extreme Density-Driven Delocalization Error for a Model Solvated-Electron System. *J. Chem. Phys.* **2013**, *139*, 184116.
(105) Rugg, G.; Genest, A.; Rösch, N. DFT Variants for Mixed-Metal Oxides. Benchmarks Using Multi-Center Cluster Models. *J. Phys. Chem. A* **2018**, *122*, 7042–7050.
(106) Löwdin, P. O. Correlation Problem in Many-Electron Quantum Mechanics: I. Review of

Different Approaches and Discussion of Some Current Ideas. In *Advances in Chemical Physics, v. 2*; Interscience Publishers, Inc.: New York, 1959; pp 207–322.
(107) Mok, D. K. W.; Neumann, R.; Handy, N. C. Dynamical and Nondynamical Correlation. *J. Phys. Chem.* **1996**, *100*, 6225–6230.
(108) Handy, N. C.; Cohen, A. J. Left-Right Correlation Energy. *Mol. Phys.* **2001**, *99* (5), 403–412.
(109) Hollett, J. W.; Gill, P. M. W. The Two Faces of Static Correlation. *J. Chem. Phys.* **2011**, *134*, 114111.
(110) Gagliardi, L.; Truhlar, D. G.; Manni, G. L.; Carlson, R. K.; Hoyer, C. E.; Bao, J. L. Multiconfiguration Pair-Density Functional Theory: A New Way To Treat Strongly Correlated Systems. *Acc. Chem. Res.* **2017**, *50*, 66–73.
(111) Hättig, C.; Klopper, W.; Köhn, A.; Tew, D. P. Explicitly Correlated Electrons in Molecules. *Chem. Rev.* **2012**, *112*, 4–74.
(112) Harvey, J. N. On the Accuracy of Density Functional Theory in Transition Metal Chemistry. *Annu. Reports Prog. Chem. - Sect. C* **2006**, *102*, 203–226.
(113) Cramer, C. J.; Truhlar, D. G. Density Functional Theory for Transition Metals and Transition Metal Chemistry. *Phys. Chem. Chem. Phys.* **2009**, *11*, 10757–10816.
(114) Neese, F. Prediction of Molecular Properties and Molecular Spectroscopy with Density Functional Theory: From Fundamental Theory to Exchange-Coupling. *Coord. Chem. Rev.* **2009**, *253*, 526–563.
(115) Tsuneda, T.; Hirao, K. Self-Interaction Corrections in Density Functional Theory. *J. Chem. Phys.* **2014**, *140*, 18A513.
(116) Polo, V.; Kraka, E.; Cremer, D. Electron Correlation and the Self-Interaction Error of Density Functional Theory. *Mol. Phys.* **2002**, *100* (11), 1771–1790.
(117) Lundberg, M.; Siegbahn, P. E. M. Quantifying the Effects of the Self-Interaction Error in DFT: When Do the Delocalized States Appear? *J. Chem. Phys.* **2005**, *122*, 224103.
(118) Cohen, A. J.; Mori-Sánchez, P.; Yang, W. T. Insights into Current Limitations of Density Functional Theory. *Science.* **2008**, *321* (5890), 792–794.
(119) Gräfenstein, J.; Cremer, D. The Self-Interaction Error and the Description of Non-Dynamic Electron Correlation in Density Functional Theory. *Theor. Chem. Acc.* **2009**, *123*, 171–182.
(120) Bao, J. L.; Gagliardi, L.; Truhlar, D. G. Self-Interaction Error in Density Functional Theory: An Appraisal. *J. Phys. Chem. Lett.* **2018**, *9*, 2353–2358.
(121) Gani, T. Z. H.; Kulik, H. J. Where Does the Density Localize? Convergent Behavior for Global Hybrids, Range Separation, and DFT+U. *J. Chem. Theory Comput.* **2016**, *12*, 5931–5945.
(122) Zhao, Q.; Kulik, H. J. Where Does the Density Localize in the Solid State? Divergent Behavior for Hybrids and DFT+U. *J. Chem. Theory Comput.* **2018**, *14*, 670–683.
(123) Grimme, S.; Hansen, A.; Brandenburg, J. G.; Bannwarth, C. Dispersion-Corrected Mean-Field Electronic Structure Methods. *Chem. Rev.* **2016**, *116*, 5105–5154.
(124) Grimme, S. Semiempirical GGA-Type Density Functional Constructed with a Long-Range Dispersion Correction. *J. Comput. Chem.* **2006**, *27*, 1787–1799.
(125) Zhao, Y.; Truhlar, D. G. The M06 Suite of Density Functionals for Main Group Thermochemistry, Thermochemical Kinetics, Noncovalent Interactions, Excited States, and Transition Elements: Two New Functionals and Systematic Testing of Four M06-Class Functionals and 12 Other Functionals. *Theor. Chem. Acc.* **2008**, *120*, 215–241.

(126) Truhlar, D. G. Dispersion Forces: Neither Fluctuating Nor Dispersing. *J. Chem. Educ.* **2019**, *2*, [Online early access]. DOI: 10.1021/acs.jchemed.8b.
(127) Raghavachari, K.; Trucks, G. W.; Pople, J. A.; Head-Gordon, M. A Fifth-Order Perturbation Comparison of Electron Correlation Theories. *Chem. Phys. Lett.* **1989**, *157* (6), 479–483.
(128) Tao, J.; Perdew, J. P.; Staroverov, V. N.; Scuseria, G. E. Climbing the Density Functional Ladder: Nonempirical Meta–Generalized Gradient Approximation Designed for Molecules and Solids. *Phys. Rev. Lett.* **2003**, *91* (14), 3–6.
(129) Chai, J.-D.; Head-Gordon, M. Long-Range Corrected Hybrid Density Functionals with Damped Atom-Atom Dispersion Corrections. *Phys. Chem. Chem. Phys.* **2008**, *10*, 6615–6620.
(130) Dinda, S.; Chiu, C.; Genest, A.; Rösch, N. Evaluation of Density Functionals for Elementary Steps of Selective Oxidation Reactions. *Comput. Theor. Chem.* **2017**, *1101*, 36–45.
(131) Asmis, K. R.; Santambrogio, G.; Brümmer, M.; Sauer, J. Polyhedral Vanadium Oxide Cages: Infrared Spectra of Cluster Anions and Size-Induced d Electron Localization. *Angew. Chemie - Int. Ed.* **2005**, *44*, 3122–3125.
(132) Becke, A. D. Density-Functional Exchange-Energy Approximation with Correct Asymptotic Behavior. *Phys. Rev. A* **1988**, *38* (6), 3098–3100.
(133) Lee, C.; Yang, W.; Parr, R. G. Development of the Colle-Salvetti Correlation-Energy Formula into a Functional of the Electron Density. *Phys. Rev. B* **1988**, *37* (2), 785–789.
(134) Becke, A. D. Density-Functional Thermochemistry. III. The Role of Exact Exchange. *J. Chem. Phys.* **1993**, *98* (7), 5648–5652.
(135) Becke, A. D. A New Mixing of Hartree-Fock and Local Density-Functional Theories. *J. Chem. Phys.* **1993**, *98*, 1372–1377.
(136) Solans-Monfort, X.; Branchadell, V.; Sodupe, M.; Sierka, M.; Sauer, J. Electron Hole Formation in Acidic Zeolite Catalysts. *J. Chem. Phys.* **2004**, *121*, 6034–6041.
(137) Rozanska, X.; Sauer, J. Oxidative Conversion of C1-C3 Alkanes by Vanadium Oxide Catalysts. DFT Results and Their Accuracy. *Int. J. Quantum Chem.* **2008**, *108*, 2223–2229.
(138) Perdew, J. P.; Burke, K.; Ernzerhof, M. Generalized Gradient Approximation Made Simple. *Phys. Rev. Lett.* **1996**, *77* (18), 3865–3868.
(139) Ciancaleoni, G.; Rampino, S.; Zuccaccia, D.; Tarantelli, F.; Belanzoni, P.; Belpassi, L. An Ab Initio Benchmark and DFT Validation Study on Gold(I)-Catalyzed Hydroamination of Alkynes. *J. Chem. Theory Comput.* **2014**, *10*, 1021–1034.
(140) Bühl, M.; Kabrede, H. Geometries of Transition-Metal Complexes from Density-Functional Theory. *J. Chem. Theory Comput.* **2006**, *2*, 1282–1290.
(141) Minenkov, Y.; Singstad, Å.; Occhipinti, G.; Jensen, V. R. The Accuracy of DFT-Optimized Geometries of Functional Transition Metal Compounds: A Validation Study of Catalysts for Olefin Metathesis and Other Reactions in the Homogeneous Phase. *Dalt. Trans.* **2012**, *41*, 5526–5541.
(142) Simón, L.; Goodman, J. M. How Reliable Are DFT Transition Structures? Comparison of GGA, Hybrid-Meta-GGA and Meta-GGA Functionals. *Org. Biomol. Chem.* **2011**, *9*, 689–700.
(143) Medvedev, M. G.; Bushmarinov, I. S.; Sun, J.; Perdew, J. P.; Lyssenko, K. A. Density Functional Theory Is Straying from the Path toward the Exact Functional. *Science.* **2017**,

355, 49–52.
(144) Peverati, R.; Truhlar, D. G. Quest for a Universal Density Functional: The Accuracy of Density Functionals across a Broad Spectrum of Databases in Chemistry and Physics. *Phil. Trans. R. Soc A.* **2014**, *372*, 20120476.
(145) Radoń, M.; Pierloot, K. Binding of CO, NO, and O_2 to Heme by Density Functional and Multireference Ab Initio Calculations. *J. Phys. Chem. A* **2008**, *112*, 11824–11832.
(146) Chen, H.; Song, J.; Lai, W.; Wu, W.; Shaik, S. Multiple Low-Lying States for Compound I of $P450_{Cam}$ and Chloroperoxidase Revealed from Multireference Ab Initio QM/MM Calculations. *J. Chem. Theory Comput.* **2010**, *6*, 940–953.
(147) Simons, M. C.; Ortuño, M. A.; Bernales, V.; Gaggioli, C. A.; Cramer, C. J.; Bhan, A.; Gagliardi, L. C-H Bond Activation on Bimetallic Two-Atom Co-M Oxide Clusters Deposited on Zr-Based MOF Nodes: Effects of Doping at the Molecular Level. *ACS Catal.* **2018**, *8* (4), 2864–2869.
(148) Vancoillie, S.; Zhao, H.; Radoń, M.; Pierloot, K. Performance of CASPT2 and DFT for Relative Spin-State Energetics of Heme Models. *J. Chem. Theory Comput.* **2010**, *6*, 576–582.
(149) Chen, H.; Lai, W.; Shaik, S. Multireference and Multiconfiguration Ab Initio Methods in Heme-Related Systems: What Have We Learned so Far? *J. Phys. Chem. B* **2011**, *115*, 1727–1742.
(150) Radoń, M.; Broclawik, E.; Pierloot, K. DFT and Ab Initio Study of Iron-Oxo Porphyrins: May They Have a Low-Lying Iron(V)-Oxo Electromer? *J. Chem. Theory Comput.* **2011**, *7*, 898–908.
(151) Radoń, M. Revisiting the Role of Exact Exchange in DFT Spin-State Energetics of Transition Metal Complexes. *Phys. Chem. Chem. Phys.* **2014**, *16*, 14479–14488.
(152) Carlson, R. K.; Odoh, S. O.; Tereniak, S. J.; Lu, C. C.; Gagliardi, L. Can Multiconfigurational Self-Consistent Field Theory and Density Functional Theory Correctly Predict the Ground State of Metal–Metal-Bonded Complexes? *J. Chem. Theory Comput.* **2015**, *11*, 4093–4101.
(153) Venturinelli Jannuzzi, S. A.; Phung, Q. M.; Domingo, A.; Formiga, A. L. B.; Pierloot, K. Spin State Energetics and Oxyl Character of Mn-Oxo Porphyrins by Multiconfigurational Ab Initio Calculations: Implications on Reactivity. *Inorg. Chem.* **2016**, *55*, 5168–5179.
(154) Phung, Q. M.; Feldt, M.; Harvey, J. N.; Pierloot, K. Toward Highly Accurate Spin State Energetics in First-Row Transition Metal Complexes: A Combined CASPT2/CC Approach. *J. Chem. Theory Comput.* **2018**, *14*, 2446–2455.
(155) Phung, Q. M.; Pierloot, K. The Dioxygen Adducts of Iron and Manganese Porphyrins: Electronic Structure and Binding Energy. *Phys. Chem. Chem. Phys.* **2018**, *20*, 17009–17019.
(156) Andersson, K.; Malmqvist, P.-Å.; Roos, B. O.; Sadlej, A. J.; Wolinski, K. Second-Order Perturbation Theory with a CASSCF Reference Function. *J. Phys. Chem.* **1990**, *94*, 5483–5488.
(157) Andersson, K.; Malmqvist, P.-A.; Roos, B. O. Second-Order Perturbation Theory with a Complete Active Space Self-Consistent Field Reference Function. *J. Chem. Phys.* **1992**, *96*, 1218–1226.
(158) Helgaker, T.; Jørgensen, P.; Olsen, J. Molecular Electronic-Structure Theory; John Wiley & Sons Ltd: Chichester, 2000; pp 1-200,433-647,724-816.
(159) Chan, G. K.-L.; Sharma, S. The Density Matrix Renormalization Group in Quantum

Chemistry. *Annual Review of Physical Chemistry*. Elsevier 2011, pp 465–481.
(160) Olsen, J. The CASSCF Method: A Perspective and Commentary. *Int. J. Quantum Chem.* **2011**, *111*, 3267–3272.
(161) Szalay, P. G.; Müller, T.; Gidofalvi, G.; Lischka, H.; Shepard, R. Multiconfiguration Self Consistent Field and Multireference Configuration Interaction Methods and Applications. *Chem. Rev.* **2012**, *112*, 108–181.
(162) Booth, G. H.; Alavi, A. Approaching Chemical Accuracy Using Full Configuration-Interaction Quantum Monte Carlo: A Study of Ionization Potentials. *J. Chem. Phys.* **2010**, *132*, 174104.
(163) Holmes, A. A.; Tubman, N. M.; Umrigar, C. J. Heat-Bath Configuration Interaction: An Efficient Selected Configuration Interaction Algorithm Inspired by Heat-Bath Sampling. *J. Chem. Theory Comput.* **2016**, *12*, 3674–3680.
(164) Evangelista, F. A. Adaptive Multiconfigurational Wave Functions. *J. Chem. Phys.* **2014**, *140*, 124114.
(165) Tubman, N. M.; Lee, J.; Takeshita, T. Y.; Head-Gordon, M.; Whaley, K. B. A Deterministic Alternative to the Full Configuration Interaction Quantum Monte Carlo Method. *J. Chem. Phys.* **2016**, *145*, 044112.
(166) Roos, B. O. The Complete Active Space Self-Consistent Field Method and Its Applications in Electronic Structure Calculations. In *Advances in Chemical Physics, v. 69: ab initio Methods in Quantum Chemistry, part II*; Lawley, K. P., Ed.; Wiley: New York, 1987; pp 399–445.
(167) Aquilante, F.; Autschbach, J.; Carlson, R. K.; Chibotaru, L. F.; Delcey, M. G.; De Vico, L.; Fdez. Galván, I.; Ferré, N.; Frutos, L. M.; Gagliardi, L.; et al. Molcas 8: New Capabilities for Multiconfigurational Quantum Chemical Calculations across the Periodic Table. *J. Comput. Chem.* **2016**, *37*, 506–541.
(168) Vogiatzis, K. D.; Ma, D.; Olsen, J.; Gagliardi, L.; De Jong, W. A. Pushing Configuration-Interaction to the Limit: Towards Massively Parallel MCSCF Calculations. *J. Chem. Phys.* **2017**, *147*, 184111.
(169) Malmqvist, P.-Å.; Rendell, A.; Roos, B. O. The Restricted Active Space Self-Consistent-Field Method, Implemented with a Split Graph Unitary Group Approach. *J. Phys. Chem.* **1990**, *94*, 5477–5482.
(170) Ma, D.; Li Manni, G.; Gagliardi, L. The Generalized Active Space Concept in Multiconfigurational Self-Consistent Field Methods. *J. Chem. Phys.* **2011**, *135*, 044128.
(171) Ivanic, J. Direct Configuration Interaction and Multiconfigurational Self-Consistent-Field Method for Multiple Active Spaces with Variable Occupations . I . Method. *J. Chem. Phys.* **2003**, *119*, 9364–9376.
(172) Bobrowicz, F. W.; Goddard III, W. A. The Self-Consistent Field Equations for Generalized Valence Bond and Open-Shell Hartree—Fock Wave Functions. In *Methods of Electronic Structure Theory*; Schaefer, H. F., Ed.; Springer: New York, 1977; pp 79–127.
(173) Odoh, S. O.; Manni, G. L.; Carlson, R. K.; Truhlar, D. G.; Gagliardi, L. Separated-Pair Approximation and Separated-Pair Pair-Density Functional Theory. *Chem. Sci.* **2016**, *7*, 2399–2413.
(174) White, S. R. Density Matrix Formulation for Quantum Renormalization Groups. *Phys. Rev. Lett.* **1992**, *69* (19), 2863–2866.
(175) White, S. R. Density-Matrix Algorithms for Quantum Renormalization Groups. *Phys. Rev.*

B **1993**, *48* (14), 10345–10356.
(176) White, S. R.; Martin, R. L. Ab Initio Quantum Chemistry Using the Density Matrix Renormalization Group. *J. Chem. Phys.* **1999**, *110*, 4127–4130.
(177) Wouters, S.; Neck, D. Van. The Density Matrix Renormalization Group for Ab Initio Quantum Chemistry. *Eur. Phys. J. D* **2014**, *68*, 272.
(178) Sharma, P.; Bernales, V.; Knecht, S.; Truhlar, D. G.; Gagliardi, L. Density Matrix Renormalization Group Pair-Density Functional Theory (DMRG-PDFT): Singlet-Triplet Gaps in Polyacenes and Polyacetylenes. *Chem. Sci.* **2019**, *10*, 1716–1723.
(179) Mizukami, W.; Kurashige, Y.; Yanai, T. More π Electrons Make a Difference: Emergence of Many Radicals on Graphene Nanoribbons Studied by *Ab Initio* DMRG Theory. *J. Chem. Theory Comput.* **2013**, *9*, 401–407.
(180) Kurashige, Y. Multireference Electron Correlation Methods with Density Matrix Renormalisation Group Reference Functions. *Mol. Phys.* **2014**, *112* (11), 1485–1494.
(181) Stein, C. J.; Reiher, M. Automated Selection of Active Orbital Spaces. *J. Chem. Theory Comput.* **2016**, *12*, 1760−1771.
(182) Keller, S.; Boguslawski, K.; Janowski, T.; Reiher, M.; Pulay, P. Selection of Active Spaces for Multiconfigurational Wavefunctions. *J. Chem. Phys.* **2015**, *142*, 244104.
(183) Bao, J. J.; Dong, S. S.; Gagliardi, L.; Truhlar, D. G. Automatic Selection of an Active Space for Calculating Electronic Excitation Spectra by MS-CASPT2 or MC-PDFT. *J. Chem. Theory Comput.* **2018**, *14*, 2017–2025.
(184) Pulay, P. A Perspective on the CASPT2 Method. *Int. J. Quantum Chem.* **2011**, *111*, 3273–3279.
(185) Malmqvist, P. Å.; Pierloot, K.; Shahi, A. R. M.; Cramer, C. J.; Gagliardi, L. The Restricted Active Space Followed by Second-Order Perturbation Theory Method: Theory and Application to the Study of CuO_2 and Cu_2O_2 Systems. *J. Chem. Phys.* **2008**, *128*, 204109.
(186) Ma, D.; Li Manni, G.; Olsen, J.; Gagliardi, L. Second Order Perturbation Theory for Generalized Active Space Self-Consistent-Field Wave Functions. *J. Chem. Theory Comput.* **2016**, *12*, 3208–3213.
(187) Kurashige, Y.; Yanai, T. Second-Order Perturbation Theory with a Density Matrix Renormalization Group Self-Consistent Field Reference Function: Theory and Application to the Study of Chromium Dimer. *J. Chem. Phys.* **2011**, *135*, 094104.
(188) Ghigo, G.; Roos, B. O.; Malmqvist, P.-Å. A Modified Definition of the Zeroth-Order Hamiltonian in Multiconfigurational Perturbation Theory (CASPT2). *Chem. Phys. Lett.* **2004**, *396*, 142–149.
(189) Zobel, J. P.; Nogueira, J. J.; González, L. The IPEA Dilemma in CASPT2. *Chem. Sci.* **2016**, *8*, 1482–1499.
(190) Ruipérez, F.; Aquilante, F.; Ugalde, J. M.; Infante, I. Complete vs Restricted Active Space Perturbation Theory Calculation of the Cr2 Potential Energy Surface. *J. Chem. Theory Comput.* **2011**, *7*, 1640–1646.
(191) Pierloot, K.; Phung, Q. M.; Domingo, A. Spin State Energetics in First-Row Transition Metal Complexes: Contribution of (3*s*3*p*) Correlation and Its Description by Second-Order Perturbation Theory. *J. Chem. Theory Comput.* **2017**, *13*, 537–553.
(192) Forsberg, N.; Malmqvist, P.-Å. Multiconfiguration Perturbation Theory with Imaginary Level Shift. *Chem. Phys. Lett.* **1997**, *274*, 196–204.
(193) Sand, A. M.; Truhlar, D. G.; Gagliardi, L. Efficient Algorithm for Multiconfiguration

Pair-Density Functional Theory with Application to the Heterolytic Dissociation Energy of Ferrocene. *J. Chem. Phys.* **2017**, *146*, 034101.
(194) Sand, A. M.; Truhlar, D. G.; Gagliardi, L. Erratum: "Efficient Algorithm for Multiconfiguration Pair-Density Functional Theory with Application to the Heterolytic Dissociation Energy of Ferrocene" [J. Chem. Phys. 146, 034101 (2017)]. *J. Chem. Phys.* **2017**, *146*, 189901.
(195) Angeli, C.; Cimiraglia, R.; Evangelisti, S.; Leininger, T.; Malrieu, J. P. Introduction of N-Electron Valence States for Multireference Perturbation Theory. *J. Chem. Phys.* **2001**, *114*, 10252.
(196) Guo, S.; Watson, M. A.; Hu, W.; Sun, Q.; Chan, G. K. L. N-Electron Valence State Perturbation Theory Based on a Density Matrix Renormalization Group Reference Function, with Applications to the Chromium Dimer and a Trimer Model of Poly(p-Phenylenevinylene). *J. Chem. Theory Comput.* **2016**, *12*, 1583–1591.
(197) Werner, H. J.; Reinsch, E. A. The Self-Consistent Electron Pairs Method for Multiconfiguration Reference State Functions. *J. Chem. Phys.* **1982**, *76*, 3144–3156.
(198) Knowles, P. J.; Werner, H. J. An Efficient Method for the Evaluation of Coupling Coefficients in Configuration Interaction Calculations. *Chem. Phys. Lett.* **1988**, *145* (6), 514–522.
(199) Werner, H. J.; Knowles, P. J. An Efficient Internally Contracted Multiconfiguration-Reference Configuration Interaction Method. *J. Chem. Phys.* **1988**, *89* (9), 5803–5814.
(200) Maier, T. M.; Boese, A. D.; Sauer, J.; Wende, T.; Fagiani, M.; Asmis, K. R. The Vibrational Spectrum of FeO^{2+} Isomers - Theoretical Benchmark and Experiment. *J. Chem. Phys.* **2014**, *140*, 204315.
(201) Gdanitz, R. J.; Ahlrichs, R. The Averaged Coupled-Pair Functional (ACPF): A Size-Extensive Modification of MR CI(SD). *Chem. Phys. Lett.* **1988**, *143* (5), 413–420.
(202) Saitow, M.; Kurashige, Y.; Yanai, T. Fully Internally Contracted Multireference Configuration Interaction Theory Using Density Matrix Renormalization Group: A Reduced-Scaling Implementation Derived by Computer-Aided Tensor Factorization. *J. Chem. Theory Comput.* **2015**, *11*, 5120–5131.
(203) Li Manni, G.; Carlson, R. K.; Luo, S.; Ma, D.; Olsen, J.; Truhlar, D. G.; Gagliardi, L. Multiconfiguration Pair-Density Functional Theory. *J. Chem. Theory Comput.* **2014**, *10*, 3669−3680.
(204) Stoneburner, S. J.; Truhlar, D. G.; Gagliardi, L. MC-PDFT Can Calculate Singlet-Triplet Splittings of Organic Diradicals. *J. Chem. Phys.* **2018**, *148* (6), 064108.
(205) Bao, J. L.; Wang, Y.; He, X.; Gagliardi, L.; Truhlar, D. G. Multiconfiguration Pair-Density Functional Theory Is Free from Delocalization Error. *J. Phys. Chem. Lett.* **2017**, *8*, 5616–5620.
(206) Sharma, P.; Truhlar, D. G.; Gagliardi, L. Multiconfiguration Pair-Density Functional Theory Investigation of the Electronic Spectrum of MnO_4^-. *J. Chem. Phys.* **2018**, *148*, 124305.
(207) Carlson, R. K.; Truhlar, D. G.; Gagliardi, L. Multiconfiguration Pair-Density Functional Theory: A Fully Translated Gradient Approximation and Its Performance for Transition Metal Dimers and the Spectroscopy of $Re_2Cl_8^{2-}$. *J. Chem. Theory Comput.* **2015**, *11*, 4077–4085.
(208) Carlson, R. K.; Li Manni, G.; Sonnenberger, A. L.; Truhlar, D. G.; Gagliardi, L. Multiconfiguration Pair-Density Functional Theory: Barrier Heights and Main Group and

Transition Metal Energetics. *J. Chem. Theory Comput.* **2015**, *11*, 82–90.
(209) Carlson, R. K.; Li Manni, G.; Sonnenberger, A. L.; Truhlar, D. G.; Gagliardi, L. Correction to Multiconfiguration Pair-Density Functional Theory: Barrier Heights and Main Group and Transition Metal Energetics. *J. Chem. Theory Comput.* **2016**, *12*, 457.
(210) Bao, J. L.; Odoh, S. O.; Gagliardi, L.; Truhlar, D. G. Predicting Bond Dissociation Energies of Transition-Metal Compounds by Multiconfiguration Pair-Density Functional Theory and Second-Order Perturbation Theory Based on Correlated Participating Orbitals and Separated Pairs. *J. Chem. Theory Comput.* **2017**, *13*, 616–626.
(211) Sharkas, K.; Gagliardi, L.; Truhlar, D. G. Multiconfiguration Pair-Density Functional Theory and Complete Active Space Second Order Perturbation Theory. Bond Dissociation Energies of FeC, NiC, FeS, NiS, FeSe, and NiSe. *J. Phys. Chem. A* **2017**, *121*, 9392–9400.
(212) Wilbraham, L.; Verma, P.; Truhlar, D. G.; Gagliardi, L.; Ciofini, I. Multiconfiguration Pair-Density Functional Theory Predicts Spin-State Ordering in Iron Complexes with the Same Accuracy as Complete Active Space Second-Order Perturbation Theory at a Significantly Reduced Computational Cost. *J. Phys. Chem. Lett.* **2017**, *8*, 2026–2030.
(213) Zhou, C.; Gagliardi, L.; Truhlar, D. G. Multiconfiguration Pair-Density Functional Theory for Iron Porphyrin with CAS, RAS, and DMRG Active Spaces. *J. Phys. Chem. A* **2019**, *123*, 3389–3394.
(214) Bao, J. L.; Zhang, X.; Xu, X.; Truhlar, D. G. Predicting Bond Dissociation Energy and Bond Length for Bimetallic Diatomic Molecules: A Challenge for Electronic Structure Theory. *Phys. Chem. Chem. Phys.* **2017**, *19*, 5839–5854.
(215) Stoneburner, S. J.; Livermore, V.; McGreal, M. E.; Yu, D.; Vogiatzis, K. D.; Snurr, R. Q.; Gagliardi, L. Catechol-Ligated Transition Metals: A Quantum Chemical Study on a Promising System for Gas Separation. *J. Phys. Chem. C* **2017**, *121*, 10463–10469.
(216) Kurashige, Y.; Chan, G. K. L.; Yanai, T. Entangled Quantum Electronic Wavefunctions of the Mn_4CaO_5 Cluster in Photosystem II. *Nat. Chem.* **2013**, *5*, 660–666.
(217) Altun, A.; Breidung, J.; Neese, F.; Thiel, W. Correlated Ab Initio and Density Functional Studies on H_2 Activation by FeO^+. *J. Chem. Theory Comput.* **2014**, *10*, 3807–3820.
(218) Singh, S. K.; Atanasov, M.; Neese, F. Challenges in Multireference Perturbation Theory for the Calculations of the G-Tensor of First-Row Transition-Metal Complexes. *J. Chem. Theory Comput.* **2018**, *14* (9), 4662–4677.
(219) Van Stappen, C.; Maganas, D.; Debeer, S.; Bill, E.; Neese, F. Investigations of the Magnetic and Spectroscopic Properties of V(III) and V(IV) Complexes. *Inorg. Chem.* **2018**, *57*, 6421–6438.
(220) Delcey, M. G.; Pierloot, K.; Phung, Q. M.; Vancoillie, S.; Lindh, R.; Ryde, U. Accurate Calculations of Geometries and Singlet-Triplet Energy Differences for Active-Site Models of [NiFe] Hydrogenase. *Phys. Chem. Chem. Phys.* **2014**, *16*, 7929–7938.
(221) Retegan, M.; Krewald, V.; Mamedov, F.; Neese, F.; Lubitz, W.; Cox, N.; Pantazis, D. A. A Five-Coordinate Mn(IV) Intermediate in Biological Water Oxidation: Spectroscopic Signature and a Pivot Mechanism for Water Binding. *Chem. Sci.* **2016**, *7*, 72–84.
(222) Ye, S.; Xue, G.; Krivokapic, I.; Petrenko, T.; Bill, E.; Que, L.; Neese, F. Magnetic Circular Dichroism and Computational Study of Mononuclear and Dinuclear Iron(IV) Complexes. *Chem. Sci.* **2015**, *6*, 2909–2921.
(223) Chakraborty, U.; Demeshko, S.; Meyer, F.; Rebreyend, C.; de Bruin, B.; Atanasov, M.; Neese, F.; Mühldorf, B.; Wolf, R. Electronic Structure and Magnetic Anisotropy of an Unsaturated Cyclopentadienyl Iron(I) Complex with 15 Valence Electrons. *Angew.*

Chemie - Int. Ed. **2017**, *56*, 7995–7999.
(224) Dong, G.; Phung, Q. M.; Hallaert, S. D.; Pierloot, K.; Ryde, U. H_2 Binding to the Active Site of [NiFe] Hydrogenase Studied by Multiconfigurational and Coupled-Cluster Methods. *Phys. Chem. Chem. Phys.* **2017**, *19*, 10590–10601.
(225) Sharma, A.; Roemelt, M.; Reithofer, M.; Schrock, R. R.; Hoffman, B. M.; Neese, F. EPR/ENDOR and Theoretical Study of the Jahn-Teller-Active [HIPTN_3N]MoVL Complexes (L = N^-, NH). *Inorg. Chem.* **2017**, *56*, 6906–6919.
(226) Dong, G.; Phung, Q. M.; Pierloot, K.; Ryde, U. Reaction Mechanism of [NiFe] Hydrogenase Studied by Computational Methods. *Inorg. Chem.* **2018**, *57*, 15289–15298.
(227) Mondal, B.; Neese, F.; Bill, E.; Ye, S. Electronic Structure Contributions of Non-Heme Oxo-Iron(V) Complexes to the Reactivity. *J. Am. Chem. Soc.* **2018**, *140*, 9531–9544.
(228) Kurashige, Y.; Saitow, M.; Chalupský, J.; Yanai, T. Radical O-O Coupling Reaction in Diferrate-Mediated Water Oxidation Studied Using Multireference Wave Function Theory. *Phys. Chem. Chem. Phys.* **2014**, *16*, 11988–11999.
(229) Yanai, T.; Tew, D. P.; Handy, N. C. A New Hybrid Exchange-Correlation Functional Using the Coulomb-Attenuating Method (CAM-B3LYP). *Chem. Phys. Lett.* **2004**, *393*, 51–57.
(230) Perdew, J. P. Density-Functional Approximation for the Correlation Energy of the Inhomogeneous Electron Gas. *Phys. Rev. B* **1986**, *33* (12), 8822–8824.
(231) Grimme, S. Semiempirical Hybrid Density Functional with Perturbative Second-Order Correlation. *J. Chem. Phys.* **2006**, *124*, 034108.
(232) Pykavy, M.; Van Wüllen, C.; Sauer, J. Electronic Ground States of the $V_2O_4^{+/0/-}$ Species from Multireference Correlation and Density Functional Studies. *J. Chem. Phys.* **2004**, *120* (9), 4207–4215.
(233) King, A. E.; Nippe, M.; Atanasov, M.; Chantarojsiri, T.; Wray, C. A.; Bill, E.; Neese, F.; Long, J. R.; Chang, C. J. A Well-Defined Terminal Vanadium(III) Oxo Complex. *Inorg. Chem.* **2014**, *53*, 11388–11395.
(234) Rezabal, E.; Ruipérez, F.; Ugalde, J. M. Quantum Chemical Study of the Catalytic Activation of Methane by Copper Oxide and Copper Hydroxide Cations. *Phys. Chem. Chem. Phys.* **2013**, *15*, 1148–1153.
(235) Zhao, Y.; Truhlar, D. G. Density Functionals with Broad Applicability in Chemistry. *Acc. Chem. Res.* **2008**, *41*, 157–167.
(236) Szilagyi, R. K.; Metz, M.; Solomon, E. I. Spectroscopic Calibration of Modern Density Functional Methods Using $[CuCl_4]^{2-}$. *J. Phys. Chem. A* **2002**, *106*, 2994–3007.
(237) Vogiatzis, K. D.; Li, G.; Hensen, E. J. M.; Gagliardi, L.; Pidko, E. A. Electronic Structure of the $[Cu_3(\mu\text{-}O)_3]^{2+}$ Cluster in Mordenite Zeolite and Its Effects on the Methane to Methanol Oxidation. *J. Phys. Chem. C* **2017**, *121*, 22295–22302.
(238) Snyder, B. E. R.; Vanelderen, P.; Bols, M. L.; Hallaert, S. D.; Böttger, L. H.; Ungur, L.; Pierloot, K.; Schoonheydt, R. A.; Sels, B. F.; Solomon, E. I. The Active Site of Low-Temperature Methane Hydroxylation in Iron-Containing Zeolites. *Nature* **2016**, *536*, 317–321.
(239) Hallaert, S. D.; Bols, M. L.; Vanelderen, P.; Schoonheydt, R. A.; Sels, B. F.; Pierloot, K. Identification of α-Fe in High-Silica Zeolites on the Basis of Ab Initio Electronic Structure Calculations. *Inorg. Chem.* **2017**, *56*, 10681–10690.
(240) Bols, M. L.; Hallaert, S. D.; Snyder, B. E. R.; Devos, J.; Plessers, D.; Rhoda, H. M.; Dusselier, M.; Schoonheydt, R. A.; Pierloot, K.; Solomon, E. I.; et al. Spectroscopic

Identification of the α-Fe/α-O Active Site in Fe-CHA Zeolite for the Low-Temperature Activation of the Methane C-H Bond. *J. Am. Chem. Soc.* **2018**, *140*, 12021–12032.
(241) Xiao, D. J.; Bloch, E. D.; Mason, J. A.; Queen, W. L.; Hudson, M. R.; Planas, N.; Borycz, J.; Dzubak, A. L.; Verma, P.; Lee, K.; et al. Oxidation of Ethane to Ethanol by N_2O in a Metal-Organic Framework with Coordinatively Unsaturated Iron(II) Sites. *Nat. Chem.* **2014**, *6*, 590–595.
(242) Verma, P.; Vogiatzis, K. D.; Planas, N.; Borycz, J.; Xiao, D. J.; Long, J. R.; Gagliardi, L.; Truhlar, D. G. Mechanism of Oxidation of Ethane to Ethanol at Iron(IV)–Oxo Sites in Magnesium-Diluted Fe_2(Dobdc). *J. Am. Chem. Soc.* **2015**, *137*, 5770–5781.
(243) Vogiatzis, K. D.; Haldoupis, E.; Xiao, D. J.; Long, J. R.; Siepmann, J. I.; Gagliardi, L. Accelerated Computational Analysis of Metal-Organic Frameworks for Oxidation Catalysis. *J. Phys. Chem. C* **2016**, *120*, 18707–18712.
(244) Liao, P.; Getman, R. B.; Snurr, R. Q. Optimizing Open Iron Sites in Metal-Organic Frameworks for Ethane Oxidation: A First-Principles Study. *ACS Appl. Mater. Interfaces* **2017**, *9*, 33484–33492.
(245) Vitillo, J. G.; Bhan, A.; Cramer, C. J.; Lu, C. C.; Gagliardi, L. Quantum Chemical Characterization of Structural Single Fe(II) Sites in MIL-Type Metal–Organic Frameworks for the Oxidation of Methane to Methanol and Ethane to Ethanol. *ACS Catal.* **2019**, *9*, 2870–2879.
(246) Bernales, V.; League, A. B.; Li, Z.; Schweitzer, N. M.; Peters, A. W.; Carlson, R. K.; Hupp, J. T.; Cramer, C. J.; Farha, O. K.; Gagliardi, L. Computationally Guided Discovery of a Catalytic Cobalt-Decorated Metal-Organic Framework for Ethylene Dimerization. *J. Phys. Chem. C* **2016**, *120*, 23576–23583.
(247) Bernales, V.; League, A. B.; Li, Z.; Schweitzer, N. M.; Peters, A. W.; Carlson, R. K.; Hupp, J. T.; Cramer, C. J.; Farha, O. K.; Gagliardi, L. Correction to "Computationally Guided Discovery of a Catalytic Cobalt-Decorated Metal-Organic Framework for Ethylene Dimerization." *J. Phys. Chem. C* **2017**, *121*, 11975.
(248) Chalupsky, J.; Rokob, T. A.; Kurashige, Y.; Yanai, T.; Solomon, E. I.; Rulíšek, L.; Srnec, M. Reactivity of the Binuclear Non-Heme Iron Active Site of Δ^9 Desaturase Studied by Large-Scale Multireference Ab Initio Calculations. *J. Am. Chem. Soc.* **2014**, *136*, 15977−15991.
(249) Yang, D.; Ortuño, M. A.; Bernales, V.; Cramer, C. J.; Gagliardi, L.; Gates, B. C. Structure and Dynamics of Zr6O8 Metal-Organic Framework Node Surfaces Probed with Ethanol Dehydration as a Catalytic Test Reaction. *J. Am. Chem. Soc.* **2018**, *140*, 3751–3759.
(250) Sand, A. M.; Hoyer, C. E.; Sharkas, K.; Kidder, K. M.; Lindh, R.; Truhlar, D. G.; Gagliardi, L. Analytic Gradients for Complete Active Space Pair-Density Functional Theory. *J. Chem. Theory Comput.* **2018**, *14*, 126–138.
(251) Demissie, T. B.; Garabato, B. D.; Ruud, K.; Kozlowski, P. M. Mercury Methylation by Cobalt Corrinoids: Relativistic Effects Dictate the Reaction Mechanism. *Angew. Chemie - Int. Ed.* **2016**, *55*, 11503–11506.
(252) Gaggioli, C. A.; Belpassi, L.; Tarantelli, F.; Zuccaccia, D.; Harvey, J. N.; Belanzoni, P. Dioxygen Insertion into the Gold(I)-Hydride Bond: Spin Orbit Coupling Effects in the Spotlight for Oxidative Addition. *Chem. Sci.* **2016**, *7*, 7034–7039.
(253) Gaggioli, C. A.; Belpassi, L.; Tarantelli, F.; Harvey, J. N.; Belanzoni, P. The Ligand Effect on the Oxidative Addition of Dioxygen to Gold(I)-Hydride Complexes. *Dalt. Trans.* **2017**, *46*, 11679–11690.

(254) Gaggioli, C. A.; Belpassi, L.; Tarantelli, F.; Harvey, J. N.; Belanzoni, P. Spin-Forbidden Reactions: Adiabatic Transition States Using Spin-Orbit Coupled Density Functional Theory. *Chem. - A Eur. J.* **2017**, *24*, 5006–5015.
(255) Schröder, D.; Shaik, S.; Schwarz, H. Two-State Reactivity as a New Concept in Organometallic Chemistry. *Acc. Chem. Res.* **2000**, *33*, 139–145.
(256) Poli, R.; Harvey, J. N. Spin Forbidden Chemical Reactions of Transition Metal Compounds. New Ideas and New Computational Challenges. *Chem. Soc. Rev.* **2003**, *32*, 1–8.
(257) Harvey, J. N. Spin-Forbidden Reactions: Computational Insight into Mechanisms and Kinetics. *Wiley Interdiscip. Rev. Comput. Mol. Sci.* **2014**, *4*, 1–14.
(258) Dzik, W. I., Bohmer, W., & de Bruin, B. Multiple Spin-State Scenarios in Organometallic Reactivity. In *Spin States in Biochemistry and Inorganic Chemistry: Influence on Structure and Reactivity*; 2015; p 103.
(259) Perdew, J. P. Density Functional Theory and the Band Gap Problem. *Int. J. Quantum Chem.* **1986**, *S19*, 497–523.
(260) Yakovin, I. N.; Dowben, P. A. The Problem of the Band Gap in LDA Calculations. *Surf. Rev. Lett.* **2007**, *14* (3), 481–487.
(261) Alkauskas, A.; Broqvist, P.; Pasquarello, A. Defect Energy Levels in Density Functional Calculations: Alignment and Band Gap Problem. *Phys. Rev. Lett.* **2008**, *101*, 046405.
(262) Gatti, M.; Bruneval, F.; Olevano, V.; Reining, L. Understanding Correlations in Vanadium Dioxide from First Principles. *Phys. Rev. Lett.* **2007**, *99*, 266402.
(263) Biermann, S.; Aryasetiawan, F.; Georges, A. First-Principles Approach to the Electronic Structure of Strongly Correlated Systems: Combining the GW Approximation and Dynamical Mean-Field Theory. *Phys. Rev. Lett.* **2003**, *90*, 086402.
(264) Tomczak, J. M.; Biermann, S. Effective Band Structure of Correlated Materials: The Case of VO2. *J. Phys. Condens. Matter* **2007**, *19*, 365206.
(265) Knizia, G.; Chan, G. K. L. Density Matrix Embedding: A Simple Alternative to Dynamical Mean-Field Theory. *Phys. Rev. Lett.* **2012**, *109*, 186404.
(266) Knizia, G.; Chan, G. K. L. Density Matrix Embedding: A Strong-Coupling Quantum Embedding Theory. *J. Chem. Theory Comput.* **2013**, *9*, 1428–1432.
(267) Wouters, S.; Jiménez-Hoyos, C. A.; Sun, Q.; Chan, G. K. L. A Practical Guide to Density Matrix Embedding Theory in Quantum Chemistry. *J. Chem. Theory Comput.* **2016**, *12*, 2706–2719.
(268) Fulde, P.; Stoll, H. Dealing with the Exponential Wall in Electronic Structure Calculations. *J. Chem. Phys.* **2017**, *146*, 194107.
(269) Gunst, K.; Wouters, S.; De Baerdemacker, S.; Van Neck, D. Block Product Density Matrix Embedding Theory for Strongly Correlated Spin Systems. *Phys. Rev. B* **2017**, *95*, 195127.
(270) Ricke, N.; Welborn, M.; Ye, H. Z.; Van Voorhis, T. Performance of Bootstrap Embedding for Long-Range Interactions and 2D Systems. *Mol. Phys.* **2017**, *115* (17–18), 2242–2253.
(271) Zheng, B. X.; Kretchmer, J. S.; Shi, H.; Zhang, S.; Chan, G. K. L. Cluster Size Convergence of the Density Matrix Embedding Theory and Its Dynamical Cluster Formulation: A Study with an Auxiliary-Field Quantum Monte Carlo Solver. *Phys. Rev. B* **2017**, *95*, 045103.
(272) Kretchmer, J. S.; Chan, G. K. L. A Real-Time Extension of Density Matrix Embedding Theory for Non-Equilibrium Electron Dynamics. *J. Chem. Phys.* **2018**, *148*, 054108.

(273) Pham, H. Q.; Bernales, V.; Gagliardi, L. Can Density Matrix Embedding Theory with the Complete Activate Space Self-Consistent Field Solver Describe Single and Double Bond Breaking in Molecular Systems? *J. Chem. Theory Comput.* **2018**, *14*, 1960–1968.
(274) Hermes, M. R.; Gagliardi, L. Exactly-Embedded Multiconfigurational Self-Consistent Field Theory Using Density Matrix Embedding: The Localized Active Space Self-Consistent Field Method. *J. Chem. Theory Comput.* **2019**, *15*, 972–986.

Table of Contents Graphic